



Review article

MXene material for supercapacitor applications: A comprehensive review on properties, synthesis and machine learning for supercapacitance performance prediction



Daisy Maria Saju ^a, R. Sapna ^b, Utpal Deka ^c, K. Hareesh ^{a,*}

^a Department of Physics, Manipal Institute of Technology Bengaluru, Manipal Academy of Higher Education, Manipal, 576104, India

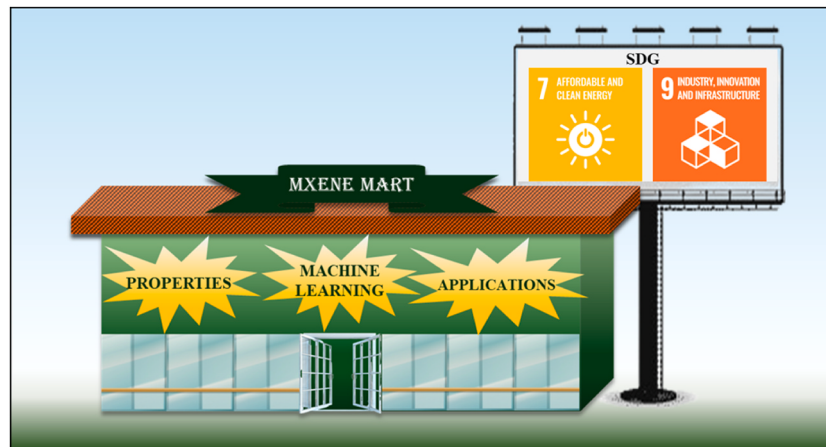
^b Department of Information Technology, Manipal Institute of Technology Bengaluru, Manipal Academy of Higher Education, Manipal, 576104, India

^c Department of Physics, Sikkim Manipal Institute of Technology, Sikkim Manipal University, Majitar, Rangpo, Sikkim, 737136, India

HIGHLIGHTS

- MXene materials for supercapacitor applications is discussed.
- MXene and their composites showed improved electrochemical performance.
- Practical applications and market analysis of supercapacitors is studied.
- ML has been used to predict the performance of supercapacitor materials.

GRAPHICAL ABSTRACT



ARTICLE INFO

Keywords:

MXene
Composites
Supercapacitor
Clean and affordable energy
Machine learning

ABSTRACT

Rapidly increasing population has raised demand for energy thus elevating the research on energy storage devices. Supercapacitors, with its wide range of features including high capacitance, high power density, and high cyclic stability has proved itself to be a remedy to the energy crisis faced globally. The advent of MXenes, a class of two-dimensional transition metal carbides or nitrides (TMCN) having excellent features including good electrical conductivity, pseudocapacitive nature and hydrophilic nature makes it as a potential material for the efficient electrode for supercapacitor application. This material offers a blend of metallic conductivity and abundant redox-active sites, therefore enabling charge storage mechanisms like electric double-layer capacitance and pseudocapacitance mechanisms contributing to clean and affordable energy. In this paper, we review the advancements in research on MXene material for supercapacitor application, including the properties, synthesis techniques of MXene ranging from HF etching to environment friendly fluoride-free approaches, MXene-based

* Corresponding author.

E-mail address: hareesh.k@manipal.edu (K. Hareesh).

materials for supercapacitor application, and much more. Additionally, ML approaches for predicting supercapacitor performance are also discussed. This review provides a holistic and forward-thinking perspective of MXenes in supercapacitor applications, addressing critical challenges and outlining future research directions that are indispensable to bridge the gap that exists between academic advancement and industrial implementation.

1. Introduction

A burgeoning populace is now seen every passing year, and this has in turn escalated the demand for energy [1]. Although there has been a great level of technological advancement and societal evolution, the demand for energy is still an ever-growing imperative. Developing sustainable energy sources is a pressing challenge, as limited availability of petroleum and the discrepancy between energy demand and renewable energy supply still persist [2,3]. This shows the relevance of research in energy storage technologies and devices.

Different energy storage devices discovered to date include batteries, fuel cells, and supercapacitors (SCs), latter being the advanced among all. The increased energy density, increased power density, less input resistance, and long life along with the prompt charge discharge makes it a promising solution to the current energy crisis faced globally [1]. The rapid surge of energy delivered by a SC can be used for initiation of a car engine or quick storage of energy released during vehicle braking. The working of a SC is a combination of battery and a conventional capacitor [3]. Batteries are energy storage devices comprised of 2 electrodes with varying chemical potential and an electrolyte [4]. Upon connecting these electrodes to an external device, there is sudden movement of electrons to more positive potential. This movement of ions through the electrolyte eventually results in tapping of electrical energy. It is observed that battery has an energy density which is 10 times more than that of SC, whereas battery's power density is 20 times less than the predicted output of a SC [5]. SCs exhibit high power density, extended cycling life, and shorter time for charging when compared to Li-ion batteries. But, batteries possess higher energy density as well as wider potential window [6]. Thus, combination of SC with battery or other power sources can be a promising solution to the challenges mentioned above. Two electrodes sandwiching a dielectric between them constitutes a conventional capacitor [7]. Conventional capacitors can be either dielectric capacitors or electrolytic capacitors [8]. There is accumulation of cations and anions at the interfacial region of electrode and electrolyte. The capacitance scales with the electrode's surface area and decreases with greater distance in between them. Electrolytic capacitors have on the order of millifarads (mF) whereas in case of dielectric capacitors it will be in microfarad (μ F) range due to limitation in number of movable electrons compared to the former one. The schematic of a SC is present in Fig. 1(a). In case of SCs, capacitance can arise either through electrochemical adsorption and desorption of ionic species or due to surface faradaic redox reactions, leading to a classification in SCs [9].

Based on mechanism involved in charge storage, SC can be categorised into three categories, electric double layer capacitor (EDLC), Pseudocapacitor (PC), and hybrid SC as seen in Fig. 1(b) [10]. A different kind of SC that has been developed recently is the "integrated SC" where a single electrode, containing positive and negative materials, can work under potential window scanning from positive to negative and can also involve different mechanisms that will result in increased capacitance and broader potential window [6]. Optimizing SCs for better performance is important and this includes discovering new materials as electrodes or electrolytes and modifying existing materials. Electrolyte, being the ionic conductor between the electrodes of a SC, majorly influences the electrochemical properties of a SC like potential window and cycle stability [11]. Various electrolytes such as aqueous electrolytes, organic electrolytes, solid-state electrolytes, and hybrid electrolytes are present with each possessing its own merits and

demerits. While aqueous electrolytes have better conductivity, organic electrolytes have high voltage window. The advantages of all this are combined in hybrid electrolyte. Developing efficient electrode materials with enhanced specific surface area (SSA), less toxicity, more resistance to corrosion, better chemical stability and environment friendly is crucial as it affects the specific capacitance (C_{sp}) of the SC [10]. RuO₂ is considered the ideal SC electrode, but its use is hindered by the high cost [6]. Pseudocapacitive materials has poor electronic conductivity and lower density of power when compared to EDLC materials.

Two-dimensional materials are renowned for their significant SSA, electronic structure and its properties [12]. The most extensively studied two dimensional material is graphene after which many 2D materials were synthesised and studied including black phosphorous [13], transition metal dichalcogenides [14], transition metal oxides [15] and lots more. A material that was found not so long ago, or more precisely, discovered in 2011 by researchers in Drexel University seems to be an opportune choice for application in SC. It is called MXene [16].

MXenes, often pronounced as 'maxenes', are 2D materials of TMCN described by the general chemical formula $M_{n+1}X_nT_x$ [17]. Here, 'M' denotes early transition metals (like Sc, Mo, V, Ti, ...), 'X' signifies carbon or/and nitrogen and 'T_x' are the surface termination groups (like -OH, -F, -O, ...). Fig. 1(c) represents the elements constituting MXene. MXenes are synthesised from the $M_{n+1}AX_n$, MAX phases which are three-dimensional [16]. MAX phase are layered hexagonal structures with closely packed layers of M along with X atoms in octahedral sites between them [18]. There exists a combination of different bonds in the MAX phase among which the strongest one is the M-X bond which is a covalent directional bond. M-A and M-M bonds are weak metallic bonds. This weak M-A bond is exploited to etch only 'A' atom layers to prepare the desired MXene. The MAX phase itself possesses a wide spectrum of properties encompassing its electrical and thermal conductivity, exceptional tolerance to damage, light weightiness, and high elastic rigidity. There exist more than 130 compositions of MAX phase out of which Ti₂AlC draws most attention due to its remarkable resistance to oxidation [19]. Formation of the dense Al₂O₃ layer at high temperature contributes to the excellent oxidation resistance of Ti₃AlC₂, Ti₂AlC, and Cr₂AlC. This oxide layer is thermodynamically stable and act as a barrier preventing further oxidation.

MXene family consists of mainly three atomic structures like M₂X, M₃X₂, and M₄X₃ [20]. Later another atomic structure, M_{1.3}X was added to the same [21]. The suffix 'ene' added resembles the similarities of its properties to that of graphene [19]. MXene with the combined properties of ceramics and metals show immense applications in lithium-ion batteries, biomedicine, lubricants, and SCs [22]. Ceramic properties include its high chemical stability enhancing the lifetime as well as reliability of all the devices, high mechanical strength strengthening the cycling stability of the batteries and SC, high thermal stability ensuring consistency in performance of SCs. High electrical conductivity and tuneable electronic properties add up as the metallic properties of the material. Most frequently studied MXenes in the arena of capturing and converting energy include Ti₄N₃T_x, Ti₂CT_x, Zr₃C₂T_x, V₄C₃T_x, Cr₂CT_x, and Nb₄C₃T_x [1]. Fig. 1(d) shows the advancement in research about MXenes used in SC applications.

MXenes have garnered significant attention for incorporation in SCs and microsupercapacitors (MSCs) [23]. MXene materials have been integrated into textile SCs, flexible Zn-ion MSCs, and nanocomposite-based SCs leading to notable advancements in capacitance, mechanical flexibility, cycling stability, and energy density

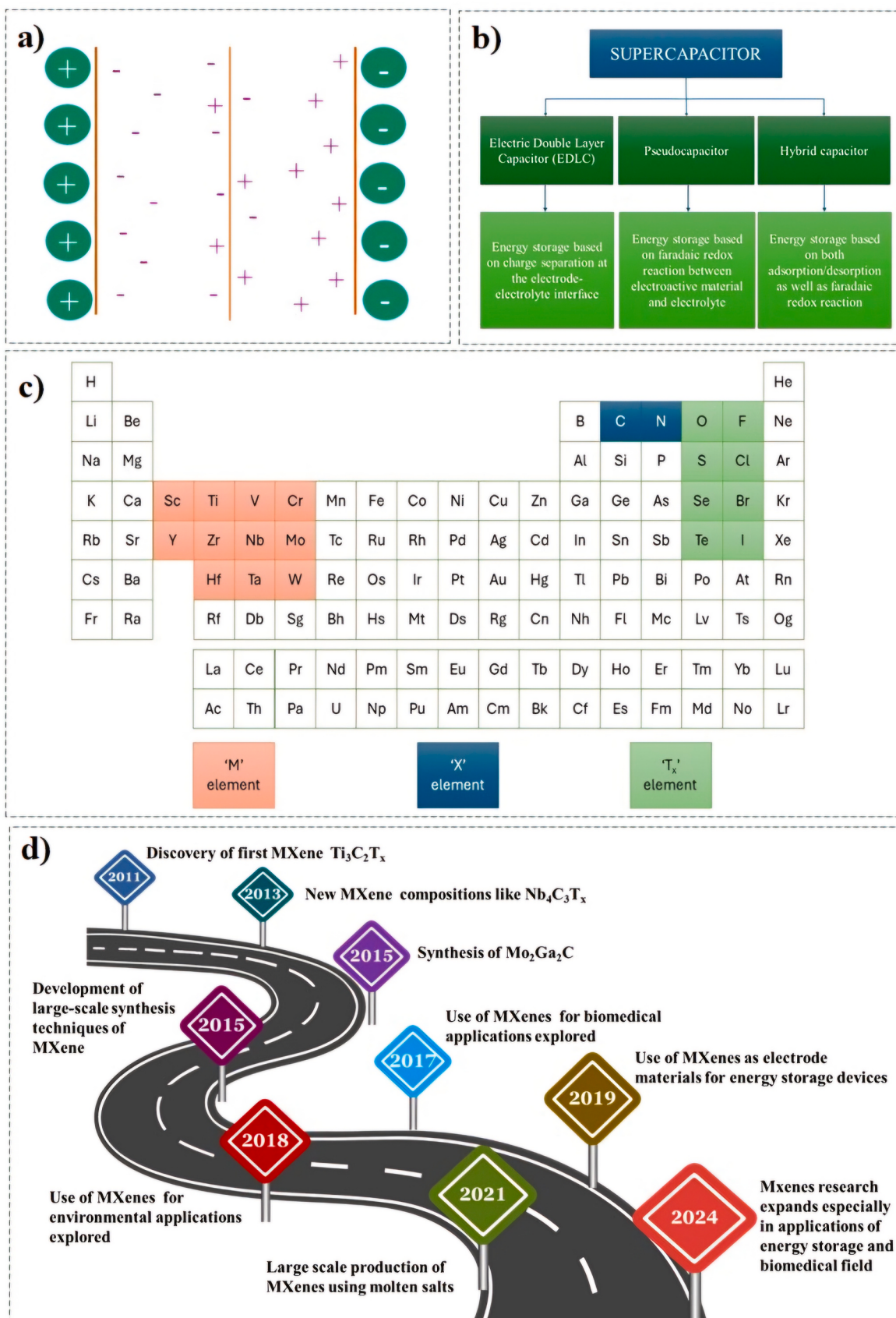


Fig. 1. a) Schematic representation of a supercapacitor b) Types of supercapacitor c) Periodic table representation of elements constituting MXene d) Timeline of progress in research on MXene.

showcasing its versatility in energy storage sector.

2. Properties of MXenes

2.1. Mechanical properties

Mechanical properties possessed by MXene are a result of the robust covalent bond existing amid the transition metal atom and the C or N atom [21]. After Al atoms are eliminated from the precursor, the MAX phase, the strength of the M-X bond increases, and this results in high elastic constant which decreases after functionalization as deformation is caused. It is also observed that carbide-based MXenes have lower Young's modulus when compared to nitride-based MXenes owing to lower electronegativity of carbon in comparison with nitrogen. Surface termination greatly affects the strength of the M – N and M – C bond [16]. Zha et al. [24] demonstrates how oxygen terminated MXenes turn preferential for application in SCs because of their high mechanical strength. At the same time, conductivity in MXenes with oxygen termination (-O) are observed to be less compared to hydroxyl terminated (-OH) MXenes [25]. This can be attributed to the strong covalent bond formation between oxygen and the transition metal resulting in lowering the number of free electrons for conduction.

2.2. Structural properties

In a MXene, 'M' atoms exist in hexagonal lattice structure whose octahedral voids are filled with 'X' atoms. It is found that MXenes mainly exist in six different structures as summarized in Table 1.

The index 'n' is crucial in determining the molecular pattern of MXene. As n index increase, instability of the MXene also increases. It was also observed that 'T' atoms being in a different position from the 'M' and 'x' atom results in highly stable configuration. MXene basically exist in three different types, namely, M_2X , M_3X_2 , and M_4X_3 . Hexagonal close-packing structure (ABABAB) is observed in M_2X whereas face-centred cubic structure (ABCABCABC) is seen in M_3X_2 and M_4X_3 MXene [26].

Thickness of the sheet influences the efficiency of SC. On studying MXene flakes ranging in size from $0.1\text{ }\mu\text{m}$ to $5\text{ }\mu\text{m}$, it was observed that highest capacitance of 290 F/g was acquired at $1\text{ }\mu\text{m}$ [27].

2.3. Electronic properties

Surface termination group ' T_x ' plays crucial role in defining the electronic behaviour of the MXene. Pristine MXene material act as metallic conductors, resembling the MAX phase whereas upon the introduction of the functional group it acquires a semiconducting nature [18]. Thus, varying surface functional groups can help in tuning its electronic properties [28]. Naguib et al. [17] studied band structure as well as electronic density of states (DOS) of MXenes using density functional theory (DFT) and obtained results which concurred with the above observation. Underminated Ti_3C_2 MXene acted as metallic conductor but, band gap with values 0.05 eV and 0.1 eV were observed in -F terminated and -OH terminated MXene respectively. The application of MXene also depends on the band gap value. Smaller band gap can ensure high mobility of electron which is very crucial for rapid

charge-discharge cycles in a SC. In other words, decrease in band gap value ensures high power density whereas increase in band gap reduce the efficiency of electron transfer, thus causing a decline in capacitance.

The exterior layer of the transition metal also has an important role in determining the electronic properties [18]. On replacing the outer Ti layers present in $Ti_3C_2(OH)_2$ with Mo atom to form $Mo_2TiC_2(OH)_2$, metallic nature shifts to semi conducting nature and a band gap valued 0.05 eV was observed [29]. Electronic properties also depend on how many layers exist, i.e., thickness of the MXene crystal. Hong et al. [30] discovered indirect band gap values of single layer MXenes and Zhou et al. [31] reported the values of band gap possessed by double layer MXenes and the latter was found to be less than single layered ones. Even conductivity between MXene layer influences the electronic behaviour of MXene [32].

2.4. Optical properties

Two-dimensional MXenes exhibit wide range of optical properties like reflectivity, transmission, refractive index, and absorption [18]. It was observed that the $Ti_3C_2T_x$ MXene shows 77% transmittance at 550 nm wavelength range [33] and 91.2% transmittance at around $300\text{--}500\text{ nm}$ wavelength range [21]. This indicates that MXenes are apt for applications in photocatalytic, photoconductive and optoelectronics field. The best possible strategy to optimize the optical characteristics of MXenes is varying the surface termination groups in it. Shahzad et al. [16] suggests that changing thickness of MXene and intercalating ions within MXene layers can enhance the transmittance percentage. Hydrazine, DMSO, and urea decreased the transmittance of $Ti_3C_2T_x$ film while tetramethyl ammonium hydroxide improved from 75% to 92% .

2.5. Stability of MXenes

Exposure to oxygen, moisture, high temperature, UV radiation can all result in the degradation of MXenes [34]. $Ti_3C_2T_x$ was found to degrade to TiO_2 when exposed to oxygen, starting from edges of MXene flake [35]. Due to this reason, it was observed that smaller flakes show faster oxidation when compared to larger ones. Increased temperature can escalate the oxidation process resulting in rapid decomposition of MXene. Photocatalytic reactions induced from exposure to UV radiation may generate oxygen containing species, thus accelerating the degradation. Concentration of the dispersed liquid is very important in determining the stability of MXene. Even the use of etching agents like hydrofluoric acid or water adds to this [21]. MXenes, being hydrophilic in nature, is well dispersed in organic solvents and it was observed that $Ti_3C_2T_x$ MXene when dispersed in water gets oxidised faster as compared to when dispersed in anhydrous isopropanol and dissolved oxygen. On comparing transition metal carbides and nitrides, carbide-based MXenes exhibit stability higher than nitride-based MXenes. Xia et al. [36] reports that rate of oxidation of MXenes can be influenced by the surrounding media too. Aqueous media aids oxidation than organic solvent or air or solid media.

Dispersion of MXenes in antioxidants also proves to be a solution to the risk of oxidation. Zhao et al. [37] and Natu et al. [38] reported use of materials that improved the antioxidant ability of MXenes. $Ti_3C_2T_x$ nanosheets dispersed in Sodium L-Ascorbate was found to retain its morphology, chemical composition, conductivity and stability for more than 21 days while in the absence of this antioxidant the nanosheet degraded to TiO_2 causing decline in conductivity [37]. Polyanions were used to cap the edges of $Ti_3C_2T_z$ and V_2CT_z nanoflakes to reduce the tendency of its oxidation when exposed to water out of which polyphosphate salts gave the best results in terms of cost effectiveness as well as eco friendliness [38]. Fabrication process too affects the stability of MXene flake, and it was found that large specific surface area flakes with less defects exhibits better environmental stability.

Table 1
Different structural forms of MXene.

Sl. No.	MXene structure	Example
1	Mono-M components	Nb_4C_3
2	Solid solutions	$(Cr,V)_3C_2$
3	Ordered out-of-plane two-fold M components	$Mo_2TiC_2T_x$
4	Ordered in-plane two-fold M components	$(Mo_{2/3}Y_{1/3})_2AlC$
5	Vacancies ordered	$Mo_{1.33}CT_x$
6	Vacancies randomly dispersed	$Nb_{1.33}CT_x$

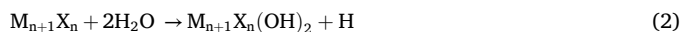
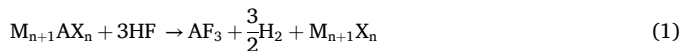
3. Synthesis of MXenes

There are many approaches to synthesis MXene materials. For example, if Ti_3SiC_2 is heated in an atmosphere rich in carbon it causes loss of Si and forms TiC_x . Heating Ti_3SiC_2 in cryolite or molten Aluminium also results in same product. Whereas heating Ti_2InC in vacuum at nearly $800^\circ C$ forms TiC_x by losing In. In short, all methods of synthesis can be separated under two broad categories namely, top-down methods and bottom-up methods.

3.1. Top-down synthesis methods

3.1.1. Hydrogen fluoride etching

The first and most common MXene, $Ti_3C_2T_x$ was prepared by selectively removing Aluminium layers in Ti_3AlC_2 by using 50 % HF solution [17]. A schematic illustration of etching is seen in Fig. 2(a). The reaction can be summarized as [1]:



Naguib et al. [39] synthesised various MXenes using HF etching method. Fig. 2(c) clearly depicts the layered $Ti_3C_2T_x$ MXene formed by HF treatment of Ti_3AlC_2 MAX phase (Fig. 2(b)). Further exfoliation can result in separation of the 2D sheets formed. Etching of Al layer is followed by reactions (2) and (3) leading to formation of surface groups like -OH or -F in MXene sheets. The process of etching is influenced by various parameters like the quality of MAX phases, etching solution, etching temperature and etching time [18]. Alhabeb et al. [20] studies the influence of concentration of HF on the concentration of surface terminations formed. Higher HF concentration results in decreased etching time which in turn increases the etching efficiency. Also, a higher HF content implies high defect concentration present in $Ti_3C_2T_x$

flakes, and this impacts the properties, quality and environmental stability of the MXenes produced. In yet another study on the influence of HF concentration on the etching process Yung et al. [40] depicts why long etching time should be avoided at higher HF concentration to prevent over etching. The composition of MAX phase determines the selection of etching condition. It was reported that higher concentration of HF is required for V-based and Nb-based MXenes than Ti-based MXenes [41].

Anayee et al. [42] in their study analysed the etching effect of HF mixed with acids like HCl and H_2SO_4 in the etching of Ti_3AlC_2 . It was found that etchants play a crucial role in the surface termination groups. HF mixed with oxidants showed an enhanced etching ability [41]. XRD results obtained after the etching of Ti_3AlC_2 using a mixture of HF and oxidants revealed that the peak (001) displaced to a smaller angle, but the introduction of oxidants increases the danger of oxidation of the synthesised MXenes [43].

3.1.2. Electrochemical etching

In this method of etching, Al atom layer in Ti_3AlC_2 MAX phase is eliminated by applying voltage with the MAX precursor as one of the electrodes [41]. Modulating etching voltage is critical for efficient removal of MAX phase. M-A bonds break when voltage is applied and with gradual increase in applied voltage A layer is progressively removed. Required MXene is formed by regulating the etching time and the voltage window. The process of etching is initially realized on the working electrode surface, and this ends in the creation of carbide derived carbon (CDC) that hinders subsequent etching. Sun et al. [44] in their work demonstrates the formation of Ti_2CT_x and CDC from the bulk MAX phase Ti_2AlC via electrochemical etching using a three-electrode setup at a voltage of 0.6 V. A setup of two-electrode with Ti_3AlC_2 MAX phase serving as working electrode as well as counter electrode was used with different electrolytes to study the influence of various electrolytes in the etching process [45]. It was observed that only Chlorine containing electrolytes ensured sufficient removal of Aluminium layer of the MAX phase. An electrochemical etching method possesses advantages of minimal usage of corrosive acid, low energy

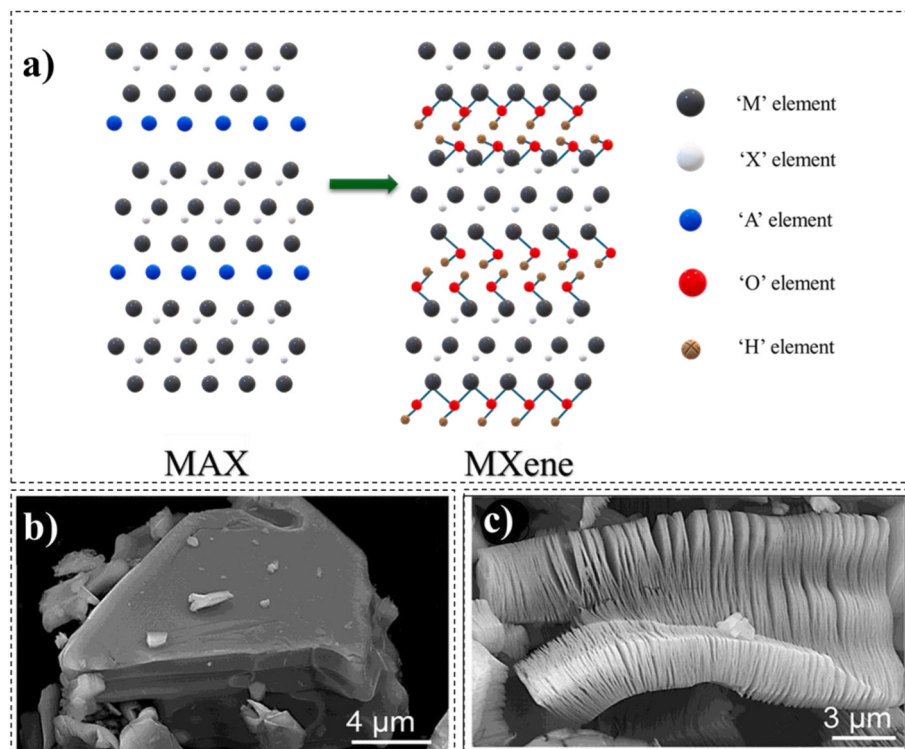


Fig. 2. a) Schematic illustration of MXene formation from MAX phase b) SEM micrograph of Ti_3AlC_2 MAX phase (c) SEM micrograph of $Ti_3C_2T_x$ MXene [39].

consumption and low reaction temperature but, the accompanying CDC layer formed results in low yield of MXene.

3.1.3. Etching using *in-situ* formed HF

Corsive nature of HF has inspired the researchers to find alternatives leading to *in-situ* HF forming techniques. Ghidu et al. [46] utilized a HCl/LiF solution to etch Ti_3AlC_2 and produced $Ti_3C_2T_x$ clay which was then rolled to a film with excellent flexibility, hydrophilicity, toughness and conductivity up to 1500 S/cm. This MXene clay when employed as working electrode for SCs, delivered a C_{sp} of 900 F/cm³ and high retention of capacitance was observed after completing 10,000 cycles. Also, intercalation of Li^+ ions resulted in expanded interlayer spacing which helps in delamination. Varying fluoride salts can adjust the interlayer spacing and studies were conducted using salts like LiF, NaF, KF and NH₄F. The variation in the composition of etchant mixture varies the morphology along with physiochemical properties of the synthesised MXene [41]. Very novel hybrid etchants like ammonium fluoride mixed with solvent of oxalic acid and choline chloride was reported by Wu et al. [47]. Even ammonium bifluoride can be used as an etching agent in this method [48]. In-Situ HF forming techniques thus provide a mild and safe method of synthesizing MXenes, but they also possess a risk of residual unetched MAX phase components.

3.1.4. Other etching techniques

Fluorine terminated MXene have lower conductivity when compared to other MXenes [34]. Also, scalability of HF etching technique is limited as this method is suitable for use only for the exfoliation of Al containing MAX phase. Moreover, HF being a very strong acid can cause serious health issues if exposed to for a long time [26]. Thus, it is important to find synthesis techniques that can yield MXene with fluorine free termination. Fluoride free molten salt is yet another etchant used for MXene synthesis. Using Lewis acid as the etchant was proposed by Li et al. [49] under the condition that melted halides with higher redox potentials can be used to etch MAX phases of a smaller redox potential. Although aqueous etching seems suitable for Aluminium containing MAX phase as well as carbide MAX phase, it is often found to fail in case of non-Al MAX phase and nitrides MAX phase [41]. Molten salts containing fluorine (like LiF, NaF, KF) at high temperature has proven as good etchants for Ti_4AlN_3 [50]. It is an efficient method to synthesize MXenes of high formation energy. A two-step etching process using an acid and alkali was proposed by Xie et al. [51]. The work involved soaking Ti_3AlC_2 in 1 M NaOH for 100 h and soaking it in 1 M H₂SO₄ for 2 h at 80 °C. Alkali helps in etching off 'A' layer atoms in MAX phase layers while acid removes the atoms in the surface. Highly concentrated alkalies can result in products that are extremely hydrophilic with fluorine free terminations but, high concentration combined with high temperature can limit the applicability of MXene.

3.1.5. Hydrothermal method

Hydrothermal technique is an environment friendly method of synthesis that helps in preparing samples with fluorine free surface terminations. Peng et al. [52] gives a detailed description of fabrication of Ti_3C_2 and Nb_2C with greater interlayer spacing and surface area using NaBF₄ and HCl. NH₄F can also be employed as etchant in hydrothermal synthesis of $Ti_3C_2T_x$ MXene from Ti_3AlC_2 MAX phase. The amount of NH₄F along with the time as well as temperature of hydrothermal etching influences the morphology of the synthesised MXene [53]. Higher concentration of impurities including AlF₃ [54] and (NH₄)₃AlF₆ [52] were also reported in this method. It was also observed in the study that at low temperature there is no etching whereas at high temperature there is chance of oxidation of prepared MXenes.

3.2. Bottom-up synthesis methods

3.2.1. Chemical vapour deposition (CVD)

CVD is another method for synthesizing ultrathin two-dimensional

transition metal carbides. Xu et al. [22] explains the making of two-dimensional ultrathin Mo₂C crystals using this method for the first time. α -Mo₂C crystals with orthorhombic crystal structure where Mo atoms have a slightly deformed hexagonal closed pack structure and C atoms occupying the octahedral voids are formed in this way. It was formed due to molten Mo-Cu alloy reacting with low concentration of CH₄ where methane acts as the source of carbon and Copper foil sitting on Molybdenum foil takes the role of substrate and the reaction takes place at a temperature above 1085 °C. Changing the experimental conditions helps in tuning the thickness and lateral size of the synthesised α -Mo₂C crystals. Increase in growth temperature resulted in rise of nucleation density whereas increase in growth time increased the crystal's lateral size. The fabricated ultrathin α -Mo₂C crystals showed excellent stability in different liquids. All the synthesised α -Mo₂C crystals were observed to be of regular shapes like triangles, rectangles and so on.

Wang et al. [55] explains the synthesis of ultrathin TaC and TaN crystals using Tantalum-Copper (Ta-Cu) bilayer and C₂H₂/NH₃ gas via CVD method. The synthesised single-crystal transition metal carbides had thickness ranging from 3 to 8 nm with a lateral size over 100 μm. At low temperature it was observed that they exhibit behaviour ranging from metallic to superconducting in nature. This varied as a function of thickness of the crystal.

3.2.2. Plasma-enhanced pulsed laser deposition (PEPLD)

PEPLD integrates Pulsed Laser Deposition with Plasma-Enhanced CVD and was reported as a method of synthesis of MXenes [56]. The amount of laser pulses helps in regulating the thickness of MXene layers. This is more efficient than CVD method as it requires simpler reaction condition and less temperature. This method was used by Zhang et al. [57] to grow Mo₂C films. 500 V of dc voltage was applied to produce plasma by ionizing methane gas at a pressure of 15 Pa and then pulsed deposition was done at 700 °C using a Krypton Fluoride laser and sapphire substrate.

A comparison of the various synthesis methods can be found in

Table 2
Comparison of different synthesis techniques.

Method	Features	Limitation
HF Etching	<ul style="list-style-type: none"> Most widely used method Complete conversion of MAX to MXene was observed 	<ul style="list-style-type: none"> Direct exposure to toxic HF acid Etching process is highly dependent on large number of factors
Electrochemical Etching	<ul style="list-style-type: none"> Large-scale synthesis of MXene is possible No direct exposure to toxic chemicals 	<ul style="list-style-type: none"> Specialized instruments required Non-uniform etching across the sample
In-Situ HF Forming Etching	<ul style="list-style-type: none"> MXenes with controlled surface termination produced No direct exposure to hazardous acids 	<ul style="list-style-type: none"> In-situ HF generation raises safety concerns Careful control of reaction conditions to be taken care of
Hydrothermal Etching	<ul style="list-style-type: none"> Avoids use of toxic chemicals Improves exfoliation and delamination of MXene layers 	<ul style="list-style-type: none"> Incomplete removal of A layer atoms of MAX phase Careful control of reaction condition required
CVD	<ul style="list-style-type: none"> Do not require MAX phase Can be applied for industrial production 	<ul style="list-style-type: none"> Specialized equipment and high-temperature reaction conditions required Controlling stoichiometry and purity is a challenge
PEPLD	<ul style="list-style-type: none"> High quality MXene films produced Do not require MAX phase Allows to control film thickness and deposition 	<ul style="list-style-type: none"> Require expensive instruments Limited scalability

Table 2.

4. MXenes for SCs

4.1. MXene composites for SCs

When utilized as electrodes for SCs, MXenes exhibit significant challenges including its low energy density, its tendency to restack, and oxidation of the synthesised products [1]. Stacking of MXene sheets can subsequently cause inadequate usage of the functional groups resulting in a decline in the supercapacitive performance [58]. Combining MXenes with other suitable materials can mitigate these barriers. It is often observed that integration of various dimensional materials (0D, 1D, 2D and 3D) results in enhanced properties lacking in usual bulk materials [58]. This is the motivation towards developing MXene composites that can be used as electrodes for SCs.

However, MXene synthesised may exhibit varying electrochemical performance in different electrolytes [59]. $\text{Ti}_3\text{C}_2\text{T}_x$, the most studied MXene, was found to exhibit better electrochemical performance in alkaline electrolytes when compared to neutral electrolytes. Csp of 92 F/g was acquired in KOH electrolyte which is higher than capacitance value of 75 F/g obtained in Na_2SO_4 electrolyte. The same MXene, $\text{Ti}_3\text{C}_2\text{T}_x$, demonstrated capacitance of 51 F/g in KOH electrolyte [60], 67 F/g in NaCl electrolyte [61], 180 F/g in Li_2SO_4 electrolyte [62], and 73 F/g in K_2SO_4 electrolyte [63]. In all the above cases the preparation of MXene was by the same HF etching method yet the capacitance value differed with respect to electrolyte. This variation can be attributed to several factors like difference in pH and conductivity of each electrolyte, or the type and size of cation in electrolyte. For instance, the ionic radius of Li^+ ion is 76 p.m. while that of K^+ ion is 138 p.m. Smaller cation can intercalate more easily thus increasing the capacitance.

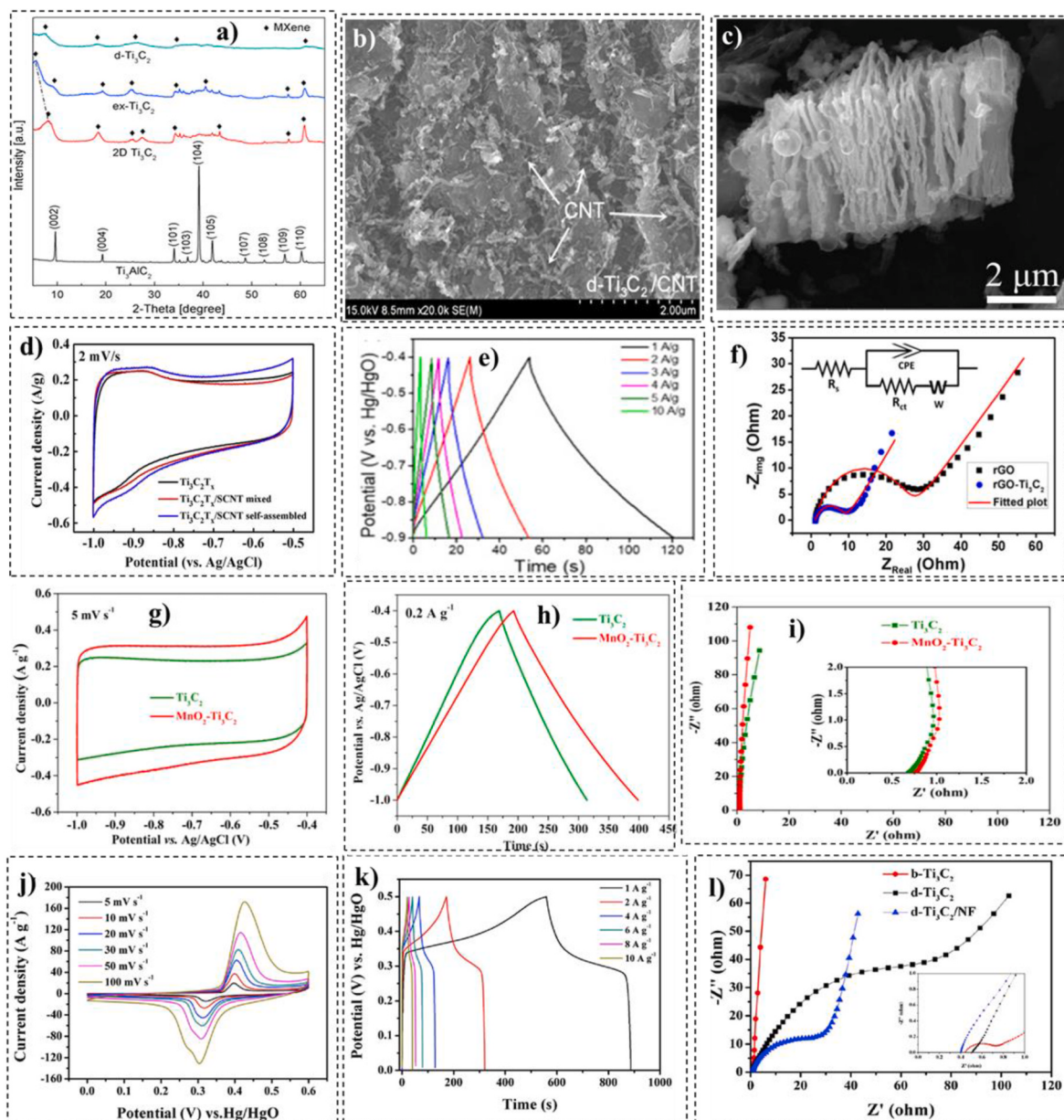


Fig. 3. a) The XRD patterns of Ti_3AlC_2 , 2D- Ti_3C_2 , and d- $\text{Ti}_3\text{C}_2/\text{CNT}$. b) SEM image of d- $\text{Ti}_3\text{C}_2/\text{CNT}$. Reproduced from Ref. [58] with the permission of Elsevier. c) SEM image of Ti_3C_2 MXene [49]. d) CV curves of the pure $\text{Ti}_3\text{C}_2\text{T}_x$ electrode, $\text{Ti}_3\text{C}_2\text{T}_x/\text{SCNT}$ composite electrode [64]. e) GCD curve of $\text{Ti}_3\text{C}_2/\text{CNTs}$ film [65]. f) Nyquist plots of rGO and rGO- Ti_3C_2 aerogel electrode [66]. g) CV curves h) GCD curves i) Nyquist plot of $\text{MnO}_2\text{-Ti}_3\text{C}_2$ electrodes. Reproduced from Ref. [72] with the permission of Elsevier. j) CV curve k) GCD curve l) Nyquist plot of d- $\text{Ti}_3\text{C}_2/\text{NF}$. Reproduced from Ref. [75] with the permission of Elsevier.

4.1.1. MXene-carbon composites

Yan et al. [58] have prepared delaminated Ti_3C_2 nanosheets by intercalation and ultrasonication and then combined it with carbon nanotubes (CNT) to prevent aggregation of the delaminated sheets. Successful synthesis of MXene and the composite was confirmed using XRD analysis as observed from Fig. 3(a). SEM micrograph of the composite is seen in Fig. 3(b). Its difference from the pristine Ti_3C_2 is very clearly understood from comparison with SEM image of Ti_3C_2 (Fig. 3(c)) obtained from Ti_3SiC_2 by molten etching method [49]. CNT increased the spacing between Ti_3C_2 sheets and this in turn improved the electrical conductivity. Different samples were made by varying the weight ratio of d- Ti_3C_2 and CNT. Maximum area of CV (cyclic voltammetry) curve was observed in the weight ratio 2:1 indicating topmost volumetric capacitance of 393 F/cm^3 at a scan rate of 5 mV/s . Comparison of CV plots of d- Ti_3C_2 and d- $\text{Ti}_3\text{C}_2/\text{CNT}$ reveals that better electrochemical performance was obtained in the composite electrode owing to the better conductivity of CNT. But it was found that restacked layers still existed in many $\text{Ti}_3\text{C}_2\text{T}_{\text{x}}/\text{CNT}$ composites.

Single-walled CNTs seemed a solution to this as $\text{Ti}_3\text{C}_2\text{T}_{\text{x}}/\text{SCNT}$ self-assembled composite electrodes exhibited greater capacitance with unit area along with cycling stability [64]. Volumetric capacitance value of 314 F/cm^3 (areal capacitance = 220 mF/cm^2) was obtained when scan rate was 2 mV/s and 205 F/cm^3 was obtained at 100 mV/s . Fig. 3(d) shows the CV plot of $\text{Ti}_3\text{C}_2\text{T}_{\text{x}}$ mixed with SCNT. Maximum area for the CV curve was observed for the $\text{Ti}_3\text{C}_2\text{T}_{\text{x}}/\text{SCNT}$ self-assembled electrode representing the maximum capacitance. Also, large slopes are observed at the beginning and the end of these curves. This shows that all electrodes have a quick response to charging and discharging. Areal capacitance was also observed to rise with increase in mass loading with maximum capacitance of 610 mF/cm^2 observed at loading of 5.6 mg/cm^2 . At the same time, Nyquist plot showed that ESR value remained invariant with mass loading while R_{ct} increased. Although CNT is a good spacer and superb conductive agent, it is often mixed with MXene by simple dispersion process and thus a sturdy method to synthesize MXene/CNT composites were yet to develop.

Yang et al. [65] explains the synthesis of $\text{Ti}_3\text{C}_2/\text{CNT}$ composites via electrophoretic deposition. This method involved simple apparatus which ensured excellent uniformity as well as mass production of electrodes without binders. Area of CV curve of CNT, Ti_3C_2 and $\text{Ti}_3\text{C}_2/\text{CNT}$ was found to increase proportionate to the scan rate and maximum area was observed for the composite. Redox peaks are also found to be absent in the curves. The GCD (Galvanostatic charging-discharging) curves of the electrode at varying current densities is seen in Fig. 3(e) and this shows that all the curves have typical triangular shape, i.e., they have good electrochemical behaviour. It can also be observed that decrease in current density leads to a rise in the charge-discharge duration and the best response is seen at current density value of 1 A/g . The electrical resistance of the electrodes was studied by performing EIS (Electrochemical Impedance Spectroscopy) and Nyquist plot was employed to calculate the solution resistance (R_s) and charge transfer resistance (R_{ct}).

Binder free, self-standing electrodes made of rGO and delaminated Ti_3C_2 sheets were synthesised to obtain high areal capacity [66]. High conductivity and greater theoretical surface area of graphene ensured promising electrochemical performance as electrodes for SC. The CV plot of rGO/ Ti_3C_2 composite electrode at various scan rates shows a symmetric current response revealing good reversibility of the electrode. GCD curve was used to calculate capacitance and areal capacitance of 171.4 mF/cm^2 (gravimetric capacitance = 190.4 F/g and volumetric capacitance = 107.1 F/cm^3) was obtained at 1 mA/cm^2 current density and 0.5625 g/cm^3 mass density. GCD plot of rGO aerogel gave 36.6 mF/cm^2 areal capacitance at 1 mA/cm^2 density of current which is nearly 4.7 times in comparison with composite electrode, thus indicating the relevance of MXene in the electrochemical characteristic of the composite electrode. EIS was also performed on the rGO electrode and the composite electrode. Nyquist plot seen in Fig. 3(f) showed a semicircle spanning high to medium frequency followed by a straight

line at high frequency. It was observed that solution resistance was same for both the electrodes while charge transfer resistance was found to be less for the electrode made of composite material. Only $4.3 \times 10^{-3} \%$ of energy loss was reported in each cycle after 1500 cycles and $2.1 \mu\text{Wh/cm}^2$ energy density was also obtained.

A very innovative composite known as BMX yarn was fabricated by bscrolling MXene with CNT [67]. CV curves were plotted for different MXene loading which clearly shows how area of curve increase with increase in loading of MXene as this results in increased number of accessible MXene sheets in yarn. GCD curves also reveals the same results. These flexible yarn electrodes with 97.4 wt% MXene loading exhibited nearly 100 % retention of capacity after 10000 cycles and volumetric capacitance of 1083 F/cm^3 at 20 mA/cm^3 . Corresponding gravimetric and linear capacitance was found to be 532 F/g and 118 mF/cm respectively. Maximum energy density of 61.6 mWh/cm^3 was also acquired when power density is 358 mW/cm^3 . This proved that using little amount of SC integrated to textile can power small electrical gadgets. Nyquist plot of the electrodes obtained after EIS showed that increase in MXene loading resulted in increase in ESR due to the increase in ion diffusion resistance as yarn becomes denser.

MXenes combined with CNT and hyaluronic acid to be used as SC electrodes was reported by Zheng et al. [68]. This hybrid fibre had high elastic modulus and tensile strength when compared to pure CNT fibres. CV curve of the MXene/CNT/HA hybrid fibre takes a quasi-rectangular shape without redox peaks suggesting EDLC behaviour of the electrode. Maximum volumetric capacitance is found to be achieved at 1:1 mass ratio of MXenes and CNT as seen in the CV plot. GCD curves of the hybrid electrode shows triangular symmetry demonstrating better coulomb efficiency and rate capability. Capacitance retention after 1000 cycles was 82.5 % while the volumetric capacitance was $13.95 \pm 2.45 \text{ F/cm}^3$. Maximum volumetric capacitance is found to be achieved at 1:1 mass ratio of MXenes and CNT.

Nitrogen-doped $\text{Nb}_2\text{CT}_{\text{x}}/\text{rGO}$ composite was developed by Nasrin et al. using supercritical fluid method [69]. Doping both rGO and $\text{Nb}_2\text{CT}_{\text{x}}$ with nitrogen using melamine formaldehyde proved useful in improving conductivity, energy storage capability, and stability. Symmetric supercapacitor fabricated using the material synthesised exhibited high capacitance of 816 F/g when current density is 2 A/g . The device also gave better energy density like 29 Wh/kg in case of aqueous H_2SO_4 electrolyte while 33 Wh/kg was obtained in non-aqueous TEABF₄/ACN electrolyte.

Li et al. [70] developed composite of $\text{Ti}_3\text{C}_2\text{T}_{\text{x}}$ MXene and electro-chemically exfoliated graphene (EG) solution processable ink for application in all-solid-state SC and in-plane MSCs. The composite combined the properties of both including high conductivity of MXene and mechanical flexibility of EG. The electrode developed demonstrated an areal capacitance of 3.26 mF/cm^2 and volumetric capacitance of 33 F/cm^3 at a scan rate of 5 mV/s . Fabricated device also demonstrated volumetric capacitance 216 F/cm^3 at 0.1 A/cm^3 . The device has also facilitated advancement towards advanced portable and microscale devices for storing energy.

4.1.2. MXene-metal oxide composites

Metal oxides and polymers possess high capacity, thus, integrating them with MXenes to synthesize composites will improve the capacitance possessed by MXene electrodes for SCs [71]. Ti_3C_2 nanosheets incorporated with MnO_2 nanoparticles showed an areal capacitance of 377 mF/cm^2 at a scan rate of 5 mV/s [72]. The CV curve obtained for the composite at 5 mV/s and GCD curve at 0.2 A/g can be seen in Fig. 3(g) and (h) respectively. MnO_2 nanoparticles have small, uniform structure that helps in increasing accessible surface area by preventing aggregation of Ti_3C_2 nanosheets. Nyquist plot of the composite obtained after EIS characterization is given in Fig. 3(i). Less charge transfer resistance and diffusion resistance were observed in MnO_2 - Ti_3C_2 electrode. In short, addition of MnO_2 to Ti_3C_2 has improved the electrochemical characteristics of pure Ti_3C_2 electrode.

NiCo_2O_4 has proven to be a potential material to be used as electrode for SCs on account of its high theoretical capacitance and good stability of charging-discharging cycling [73]. But low electronic and ionic conductivity along with easy agglomeration and the structural degradation resulting from the volume expansion during the electrochemical cycling restricts its application. Loading NiCo_2O_4 nanospheres on the surface as well as amid the layers of $\text{Ti}_3\text{C}_2\text{T}_x$ MXene has helped in overcoming these limitations as intercalation of $\text{Ti}_3\text{C}_2\text{T}_x$ MXene layers with NiCo_2O_4 nanospheres prevents the risk of agglomeration and the MXene layer acts as a layer of protection against the chance of structural damage. Wang et al. synthesised $\text{Ti}_3\text{C}_2\text{T}_x$ MXene - NiCo_2O_4 nanosphere composite and observed good rate performance along with impressive cycling stability. Later, an asymmetric capacitor with the composite material as cathode and activated carbon as anode was constructed which depicted C_{sp} of 1025 F/g at a current density of 1 A/g and energy density of 36.67 Wh/kg at a power density of 800 W/kg.

The current response here results from a mixed charge storage mechanism involving capacitive as well as diffusion-controlled processes.

$$i = k_1 v + k_2 v^{1/2} \quad (4)$$

The equation is used to calculate the contribution of each of these. Here k_1 and k_2 are surface and diffusion current, and v is the voltage sweep rate. The result of this is, as scan rate increases, the capacitance derived from diffusion control decreases indicating good capacitive nature. Highly symmetric GCD curves were obtained indicating high coulombic efficiency. Also, 82.2 % retention of capacitance was obtained at the end of 5000 cycles.

Wang et al. [74] in yet another work synthesised monolayer Ti_3C_2 MXene/ NiCo_2O_4 nanocones hybrid material and obtained mass C_{sp} of 1660.2 F/g. Then, an asymmetric SC where s- $\text{Ti}_3\text{C}_2/\text{NiCo}_2\text{O}_4$ is the positive electrode and active carbon is the C_{sp} negative electrode was fabricated and operated at a wider voltage window of 1.6 V. High C_{sp} of 73.8 F/g at a current density of 1 A/g. High energy density of 94.46 Wh/kg at a power density of 2882.0 W/kg was also obtained. SEM analysis after a long-term GCD test also showed that there was no restacking or self-aggregation of the material. Also, on calculating the diffusion-controlled mechanism contribution and capacitive mechanism to the current response indicated that there was 70.96 % capacitive contribution at a low scan rate of 1.5 mV/s which increased to 85.07 % at scan rate of 3.5 mV/s. All these features thus enhanced its potential for application in SC.

4.1.3. Other MXene composites

Guo et al. [75] formulated a method of depositing 2D MXene sheets on Ni foam to avoid reaggregation of the MXene sheets. Ni foam aids in increasing the active sites, surface area, and electrical conductivity of the MXene sheet. This composite was also capable of being directly used as a SC electrode. CV curve of the composite electrode is seen in Fig. 3(j). Increased gravimetric capacitance of 654 F/g was obtained at 1 A/g current density along with excellent cycling stability as nearly 80.6 % capacitance retention was observed in the asymmetric SC formed with d- $\text{Ti}_3\text{C}_2/\text{NF}$ positive electrode and d- Ti_3C_2 negative electrode after 5000 cycles. It also delivered energy density of 18.1 Wh/kg at power density 398 W/kg. KOH electrolyte used provides -OH, whose adsorption and desorption to the surface of Ti_3C_2 sheets causes the redox peaks seen in the CV curves.

The GCD curves (Fig. 3(k)) showed that d- $\text{Ti}_3\text{C}_2/\text{NF}$ composite has a longer charging-discharging time indicating higher charge storage capability. This confirms the results obtained from CV curve. The Nyquist plot of the electrodes was plotted after performing EIS as seen in Fig. 3(l). Solution resistance (R_s) value of d- $\text{Ti}_3\text{C}_2/\text{NF}$, obtained from the intersecting point of semicircle arc and real axis, was 0.40 Ω which was smallest among all. The charge transfer resistance (RCT), calculated from the semicircle arc in high frequency region, was also lower for the

composite compared to d- Ti_3C_2 . Thus, close contact between Ni foam and d- Ti_3C_2 sheets results in decrease of charge transfer impedance.

Somesh et al. composite of borophene with $\text{Ti}_3\text{C}_2\text{T}_x$ MXene by means of electrophoretic deposition [76]. The electrode delivered capacitance of 626.7 F/g at 1 A/g current density. It also retained 85.14 % of capacitance when density of current was increased to 20 A/g. Flexible and ultrafast SC was developed using this electrode and energy density of 75.6 Wh/kg was derived from this device.

A multidimensional heterostructure film made of 0 dimensional carbon dot, 1 dimensional carboxylated CNT, and 2 dimensional $\text{Ti}_3\text{C}_2\text{T}_x$ MXene was synthesised by Li et al. [77] to address key challenges involved in developing flexible microsupercapacitors. This combined electrode achieved a capacitance of 1162.6 mF/cm² when current density is 0.8 mA/cm² and 740.3 mF/cm² at 10 mA/cm². 107.1 % of capacitance was maintained after 10,000 cycles. Planar micro-supercapacitor was fabricated with energy density of 11.1 mWh/cm² when power density is 59.9 mW/cm². The composite has thus showed enhanced properties for application in supercapacitor including increased electrical conductivity, increased spacing between layers, and abundant porous channels.

A composite of nitrogen doped $\text{Ti}_3\text{C}_2\text{T}_x$ MXene and NiS was synthesised to develop inkjet-printing ink to be used in inkjet printing asymmetrical MSCs [78]. MXene was developed from the MAX phase using a combination of HCl and LiF as etchants, followed by annealing in nitrogen environment for developing N-doped MXene. A solvothermal method was then adopted to synthesize the composite. Wide potential window of 1.5 V was obtained along with high volumetric capacitance of 429 F/cm³ and energy density of 33.5 mWh/cm³. This has aided in increasing production efficiency. Active sites were increased, and restacking was inhibited owing to the synergistic properties of the materials. Stability of NiS had also increased.

4.2. Double transition metal MXenes

A new group of MXenes made of two transition metal elements and thus named as double transition metal (DTM) MXene was discovered in 2014 [12]. In 2014, Liu et al. [79] discovered MAX phase with new structure of the form M_3AX_2 where M composes of two transition metals Cr and Ti. $(\text{Cr}_{2/3}\text{Ti}_{1/3})_3\text{AlC}_2$ and $(\text{Cr}_{5/8}\text{Ti}_{3/8})_4\text{AlC}_3$ composed of Ti layer sandwiched between two outer layers of carbide. Developed from the corresponding MAX phase this new class of materials exhibited wide range of properties which includes high conductivity and improved chemical stability [40,80]. This led to a broad classification of MXenes into two categories as mono-M MXenes and DTM MXenes. DTM MXenes are classified as ordered and solid-solution MXenes out of which the former is further classified into in-plane MXenes and out-of-plane MXenes.

In general, a DTM MXene consists of two metals M' and M''. In case of ordered MXenes, M' and M'' fill specific sites and this is further classified as in-plane and out-of-plane MXenes [80]. In-plane ordered MXenes, known as i-MXenes, have general formula $M'_{4/3}M''_{2/3}\text{XT}_x$ where the two transition metals order alternatively in the atomic plane of each M-layer. The MXene $\text{Mo}_{4/3}\text{Y}_{2/3}\text{CT}_x$ falls under this category. Out-of-plane MXenes are represented as o-MXenes with general formula $M'_2M''_2\text{X}_3\text{T}_x$ or $M'_2M''\text{X}_2\text{T}_x$, where inner layers of M'' metal is sandwiched between outer M' layers. Examples of this include $\text{Mo}_2\text{Ti}_2\text{C}_3\text{T}_x$ and $\text{Mo}_2\text{TiC}_2\text{T}_x$. Solid-solution MXenes include two transition metals of random distribution. In all layers of M. They can be represented as $(\text{M}'\text{M}'')_{n+1}\text{C}_n\text{T}_x$ in general. Examples of solid-state MXenes include $(\text{Ti},\text{Nb})_3\text{C}_2\text{T}_x$, $(\text{Ti},\text{V})_2\text{CT}_x$, and $(\text{Nb},\text{Zr})_4\text{C}_3\text{T}_x$.

Baig et al. [81] demonstrates how electronic characteristics of a DTM MXene depend on both the transition metals present M' and M''. It was found that Ti_3CO , a mono transition metal MXene behaved like a metallic conductor while MoTiCO , a DTM MXene showed semi-conducting nature. Study on behaviour of $\text{Mo}_2\text{TiC}_2\text{T}_x$ and $\text{Mo}_2\text{Ti}_2\text{C}_3\text{T}_x$ showed that resistivity of $\text{Ti}_3\text{C}_2\text{T}_x$ decreased with decrease in

temperature while that of $\text{Mo}_2\text{TiC}_2\text{T}_x$ increased with decreasing temperature [80]. Mechanical properties too are influenced by the metals used which is evident from the investigation by Jayan et al. [82]. Upon using DFT calculation to study elastic properties of MXenes and assessing the dynamic stability parameters and elastic stiffness constant it was found that Mo-based double transition metal MXene possessed comparatively higher elasticity than Cr-based double transition metal MXene. Thermal stability of DTM MXenes was analysed through thermo-gravimetric analysis and mass spectroscopy and was found to depend on their chemical composition [80]. Hao et al. [83] observed that bare MXenes were more thermodynamically metastable with greater surface energy. Number of transition metal layers too determine the stability as stability increase with increase in layers [84].

Anasori et al. [12] predicted stability of nearly 20 DTM MXenes with general formulae $M_2'M''C_2$ and $M_2'M''C_3$ using Density Functional Theory (DFT). They observed that stability depends on the elements chosen and listed out the MXenes preferring fully ordered and partially ordered state at 0K. Mo_3C_2 and Mo_4C_3 were found to be highly unstable as Mo and C atoms prefer hexagonal structure and avoid stacking in fcc, the characteristic of MXenes. DFT results were verified by the synthesis and analysis of Mo_2TiC_2 , $\text{Mo}_2\text{Ti}_2\text{C}_3$, and Cr_2TiC_2 among which $\text{Mo}_2\text{TiC}_2\text{T}_x$ DTM MXene showed highest capacitance of 413 F/cm^3 at 2 mV/s. Synthesis of $\text{Mo}_2\text{TiC}_2\text{T}_x$ MXene was confirmed from the XRD results given in Fig. 4(a). Also, the transformation from 3D MAX phase to 2D MXene was revealed by SEM analysis as seen in Fig. 4(b) and 4(c) representing MAX and MXene respectively. Also, DFT calculations were performed to determine the influence of the constituent elements in the electronic properties of $\text{Mo}_2\text{TiC}_2\text{T}_x$. Mo-Mo d-orbitals dominate the DOS at the fermi level of $\text{Mo}_2\text{TiC}_2\text{T}_x$, indicating that Mo layers control the electronic properties of the material. Bibi et al. [85] introduced hydro-thermal approach to synthesis $\text{Mo}_2\text{Ti}_2\text{C}_3\text{T}_x$ MXene and could obtain high C_{sp} of 108.5 F/g . The CV curve of $\text{Mo}_2\text{Ti}_2\text{C}_3\text{T}_x$ formed by etching using NH_4F and HCl acid for 48 h is seen in Fig. 4(d). A three-electrode setup with H_2SO_4 as electrolyte was used for this purpose. A quasi-rectangular shape was maintained by the curve through all scan rates and C_{sp} (SC) was calculated from it using the equation

$$\text{SC} = \frac{\int I \, dV}{2mv\Delta V} \quad (5)$$

Here, numerator calculates the area under CV curve, m gives active electrode material, v refers to the scan rate, and V is the operating potential window. GCD curve was also plotted Fig. 4(e).

Both the CV and GCD plots indicates high capacitance nature of the electrode compared to other samples prepared by etching for 72 h, 24 h, and 12 h. The EIS curve for each electrode is seen in Fig. 4(f). Equivalent resistance value was determined from the starting intercept at real axis, and this was the lowest for M – 48 sample. Warburg impedance too was the lowest for M – 48 representing high ionic diffusion.

A comparison among pristine MXene, MXene-based composites, and DTM MXenes can be seen in Table 3. The comparison of C_{sp} of different MXenes and its composites is tabulated in Table 4. It is evident from the table that the MXenes based composites showed enhanced C_{sp} due to the more active sites provided the composites for the storage of charges.

5. Practical applications of SCs

SCs possess a wide range of advantages including its ability to store large amount of charge, enhanced power density, and extensive life cycle. The high power performance and good working temperature range of SC turns beneficial for public transport systems like electric buses, where they effectively support regenerative braking system and engine starts in cold weather, thus contributing to development of green transportation. On combining with batteries or fuel cells, SCs turn as excellent addendum to energy storage units. For instance, in solar cell, batteries can meet the changing demands while SCs take care of frequency regulation. Similarly, in case of wind energy too. SCs help in adjusting wind mill blades with changing wind speed [96].

Flexible textile pseudocapacitors fabricated by combination of polyaniline (PANI) and activated carbon fibre felt (ACFF) were used for developing wearable energy storage devices [3]. Limited electrical conductivity and rate performance were enhanced by incorporating carbon nanotubes (CNT) and then high areal capacitance of 5119

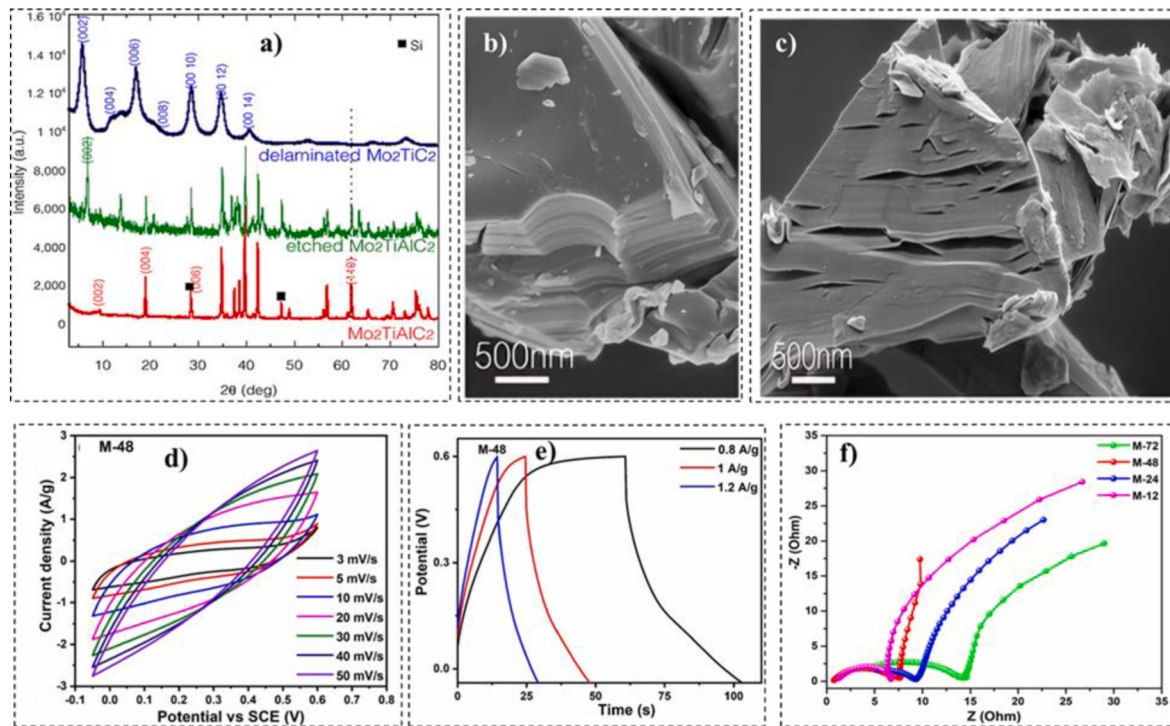


Fig. 4. a) XRD pattern of $\text{Mo}_2\text{TiAlC}_2$ and Mo_2TiC_2 . SEM image of b) $\text{Mo}_2\text{TiAlC}_2$ and c) Mo_2TiC_2 [12] d) CV curve e) GCD curve f) Nyquist plot of $\text{Mo}_2\text{Ti}_2\text{C}_3\text{T}_x$ electrode [85].

Table 3
Comparison of different kinds of MXene.

Property	Pristine MXene	MXene-based composite	DTM MXene
Structure	2 dimensional layered TMCN	Hybrid structure including MXene along with other materials like metal oxides, polymers, C-based materials and so on	2 dimensional TMCN with 2 different transition metals
Capacitance	High capacitance	Increased capacitance due to combined properties of both the materials	High capacitance owing to multiple redox active sites
Stability	Degrades over time due to oxidation	Better cycling stability due to composite reinforcement	Enhanced stability due to optimized structural stability
Interlayer spacing	Limited interlayer spacing. More chance of self-restacking	Increased interlayer spacing owing to intercalation of polymers or other materials included	Tunable interlayer spacing due to different difference in radius of metal atoms involved
Energy density	Moderate energy density	Enhanced energy density	Higher energy density than pristine MXene
Power density	Very high-power density	Slightly lower power density	Power density comparable to pristine MXenes
Synthesis	Can be synthesised by normal etching methods	Requires more complex synthesis methods	Synthesis methods are more challenging due to involvement of two transition metals

mF/cm² was observed in ACFF/PANI/CNT textile. Zhang et al. [97] proposed an electromagnetic energy harvesting system wherein energy from railroad track vibrations are collected, converted to electricity and then stored in SCs to be used as emergency or temporary power supply for rail-side equipment. Wang et al. [98] devised a nano-energy cell device with nanogenerator and SC to convert mechanical energy to electricity and then store it. Another innovative proposal was by Kindracki et al. [99] for using SC as power source for a resistojet thruster. Thrusters require large power input in short duration which is ensured

by rapid charge-discharge rate and high-power density of a SC. The electrochemical performance and high cycling capability of SCs makes it a suitable choice as power source for a resistojet thruster.

MXenes exhibit exceptional volumetric capacitance and energy density which are crucial parameters for efficient energy storage solutions in electric vehicles or portable lighting systems. The enhanced power density possessed by the material enables its application for regenerative braking in automobiles. Flexible and stretchable electrodes can be fabricated using MXene material and this is in turn beneficial for application in wearable electronics too. All these properties position them superior to the conventional electrode materials for SC applications in automobile and energy sector. Mappoli et al. [100] developed an asymmetric SC (ASC) that can overcome the limitation of low energy density and low operational voltage window possessed by usual SCs. The SCs developed had 3D printed electrodes and could operate in a wider voltage window in aqueous electrolyte. Attractive properties of Ti₃C₂T_x MXene was combined with the typical pseudocapacitive behaviour of polyaniline (PANI) to form ASC with 3D-printed nanocarbon coated with Ti₃C₂T_x as the negative electrode and 3D-printed nanocarbon electrodeposited with PANI as the positive electrode. Gel electrolyte was used to enhance mechanical stability of the device. GCD study revealed maximum areal capacitance of 24.42 mF/cm² at current density of 0.25 mA/cm². It was also observed that there was increment in capacitance to nearly 120 % of the initial capacitance value during the first 3000 cycles. Also, even after 20,000 cycles 74 % capacitance retention was observed. These results confirmed better electrochemical performance of the SC. Real-time applications of the cell were confirmed through GCD studies. It was observed that when connected in series with an LED, this SC cell turned useful in lighting the LED. Thus, this cell developed possess immense potential for energy storage applications in future. Biscrolled Ti₃C₂T_x MXene/CNT yarns (BMX) yarns were used to create high performance yarn supercapacitors (YSCs) by Wang et al. [67]. The YSC gave an energy density of 8.54 mWh/cm³ and power density of 530 mW/cm³. The BMX yarns were integrated into textile prototypes by weaving them in cotton yarn fabric as the diameter of YSC diameter was close to diameter of cotton yarn. The synthesised textile prototype demonstrated its potential in wearable electronics by powering a red LED for 60 s, a digital timer for 10 min, and a digital watch for nearly 3 h. The practical applications can be seen in Fig. 5(a) and (b). Hence, it showcased its capability of application in lighting and small electronic devices. Sun et al. [78] developed an asymmetric MSC using porous NiS/N-Ti₃C₂T_x

Table 4
Comparison of different MXene based SC electrodes.

	Electrode	Electrolyte	Csp	Method of calculation	Voltage window	Energy density	Power density	Surface area of electrode	Areal mass loading of active electrode	Reference
1	Ti ₃ C ₂ /Carbon Cloth/MnO ₂	KOH	511.2 F/g	GCD		29.58 Wh/kg	749.92 W/kg	–	–	[86]
2	Ti ₃ C ₂ /rGO	H ₂ SO ₄	140 F/g (49 mF/cm ² , 490 F/cm ³)	CV	1 V					[87]
3	Ti ₃ C ₂ /PANI	Na ₂ SO ₄	164 F/g	CV	0.6 V					[88]
4	Ti ₃ C ₂	Na ₂ SO ₄	131 F/g	CV	0.6 V					[88]
5	Ti ₃ C ₂ T _x /SWCNT	H ₂ SO ₄	1.6 mF/cm ²		0.6 V					[89]
6	Ti ₃ C ₂ T _x /C	H ₂ SO ₄	364.3 F/g	GCD	0.6 V			9 m ² /g	1 mg/cm ²	[90]
7	N-Ti ₃ C ₂	H ₂ SO ₄	2836 F/cm ³ (927 F/g)	CV	0.6 V	76 Wh/L	31112 W/L			[91]
8	Ti ₃ C ₂ T _x /rGO	H ₂ SO ₄	1040 F/cm ³	GCD	0.8 V	10.5 Wh/kg	80.3 W/kg	68.1 m ² /g		[92]
9	Ti ₃ C ₂ T _x /CNT	H ₂ SO ₄	1083 F/cm ³	GCD	0.8 V	8.54 mWh/cm ³	530 mW/cm ³			[67]
10	Ti ₃ C ₂ T _x /NiMoO ₄	KOH	1364 F/g		0.6 V	33.76 Wh/kg	400.08 W/kg	152.3 m ² /g		[93]
11	Ti ₃ C ₂ T _x	H ₂ SO ₄	542 F/g	CV	1 V	35.28 Wh/kg	18.144 kW/kg			[94]
12	Ti ₃ C ₂ /NiCo ₂ O ₄	KOH	73.8 F/g	GCD	0.7 V	94.46 Wh/kg	2882.0 W/kg	158.8 m ² /g	2.0 mg/cm ²	[74]
13	Ti ₃ C ₂ /MoS ₂	H ₂ SO ₄	386.7 F/g	GCD	0.6 V	17.4 μWh/cm ²	600 μW/kg	50.98 m ² /g		[95]

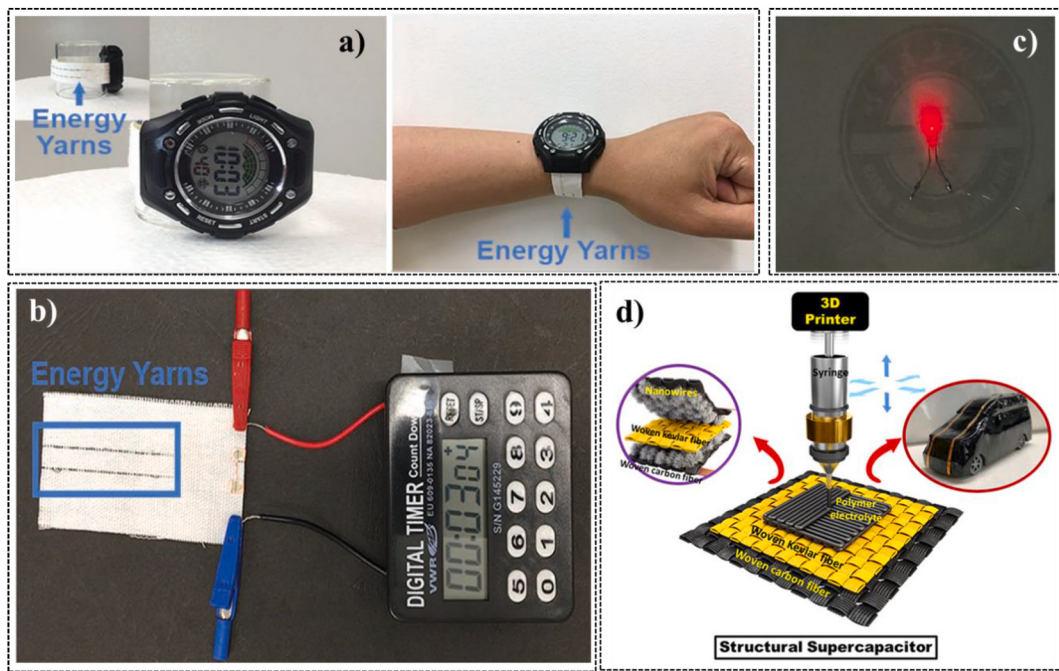


Fig. 5. Prototype of YSC device using to power a) digital watch, b) digital time. Reproduced from Ref. [67] with the permission of Wiley -VCH, c) lighting a school badge. Reproduced from Ref. [78] with the permission of Elsevier, d) Structural SC developed using N@ZnCoSe₂-MXene. Reproduced from Ref. [101] with the permission of ACS publications.

MXene as the positive electrode and rGO as the negative electrode. A pair of these devices connected in series to light a red LED attached on inkjet-printing school badge as seen in Fig. 5(c). Deka et al. [101] developed a woven carbon fibre (WCF) based SC of thermoset polyester using 3D printing. Zn-Co selenide nanowire was grown with MXenes in WCF, and this resulted in increase in the electrochemical activity of the device. The synthesised SC demonstrated high capacitance (39.11 F/g), high energy density (4.62 Wh/kg), and high power density (67.29 W/kg). The fabricated device is expected to be used in applications related to portable electronics, automotive industry, space shuttles and much more owing to its high energy density, high power density, lightweight and robust nature as well as flexibility and strength of woven carbon fibre (Fig. 5(d)).

6. Market analysis of SCs

It is very evident from literature that there is a rapid increase in energy utilization by industrial sector since 2007 that it has become the highest energy consumer in US in 2008 [102]. The current trend predicts that this demand may be doubled by the year 2050 and thus the need for efficient energy storage devices is at its peak now. SCs, with their high power density, has the ability to collect energy generated from intermittent sources and rapidly transfer them [103]. But low energy density limits the application of SC despite their large recyclability, low internal resistance or broad operation temperature range [102]. Extensive research is currently underway to discover new materials and optimize manufacturing process. To expedite time to market, it is crucial to eliminate barriers connected to cost-effectiveness, consistency of performance, and scalability. A collaboration between academia, industry, and government agencies is expected to foster research and enhance commercialization.

Commercialization of SCs began with the Gold Capacitor introduced by Panasonic and Matsushita in 1978 [104]. The capacitance value of this was from 10^{-2} F to several Farad and its operation voltage window was from 2.3 to 6 V. A concise overview of progress in commercialization of SCs is seen in Fig. 6.

At present, the primary market for SCs are small devices that are used

in consumer and industrial electronics [96]. The fast electrostatic or faradaic fast charge storing process with little volume change and long life-time ensures application of SCs from microscale devices to large-size devices, automotive transportation and much more [105]. For effective commercialization, it is crucial to boost the electrochemical activity of SCs by optimizing the factors affecting electrochemical performance of SC like SSA, surface functionalization, crystal structure, and electrode/electrolyte type.

Increased number of high diameter pores ensure greater specific surface area which in turn will contribute to improved energy density. Pores of diameter less than 0.4 nm has no contribution to capacitance. Choosing electrode materials with good stability and surface area also aids in increasing energy density and capacitance. Among the various electrolytes that exist ionic and organic electrolytes have wider operational window and efficient compatibility. Choosing the right electrolyte with respect to electrode is an important step in enhancing performance of the device.

Another significant feature in the aspect of commercialization of capacitor is developing parametric model depending on application [102]. Specifically, standard parametric model can be used for many applications, it is necessary to tune model specifically especially for military, satellite, and aircraft applications. In such instances, more non-ideal parameters like storage capacitance and resonance will have to be taken care of. Also, the voltage rating of SC being low, it becomes essential to use a series or parallel combination of SCs to ensure consistency in operation.

7. Challenges to MXene SCs

Despite being a promising material, there are numerous serious challenges possessed by MXene materials that deters their application as electrodes for SCs. Major limitations present in MXene materials can be seen in Fig. 7. At higher current densities it is often observed that MXene layers restack causing limited intercalation of cations and greater resistance to ionic diffusion in vertical direction that can deteriorate the electrochemical performance by reducing rate capability of MXene based electrode material [106]. The solution to this problem is to

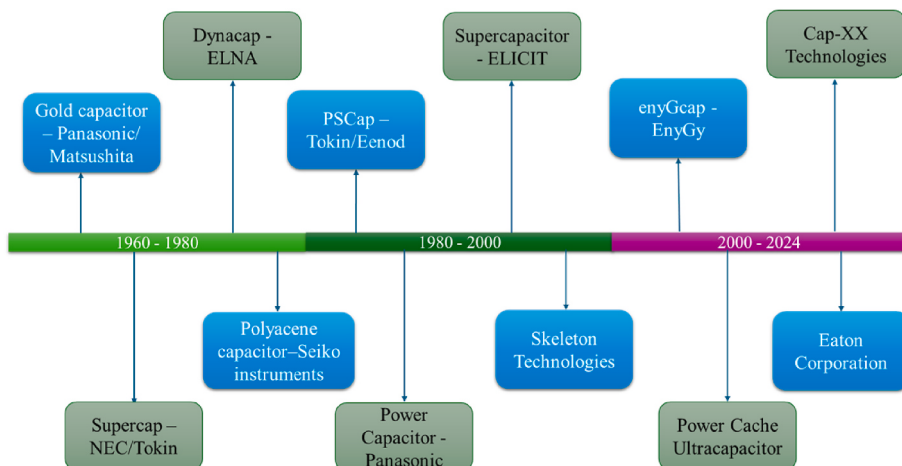


Fig. 6. Timeline of progress in commercialization of supercapacitors.



Fig. 7. Challenges of MXene-based SC.

enlarge interlayer distance by which faster and better diffusion of ions and electrolytes can be ensured. Sun et al. [107] developed an effective method to prepare flexible MXene films through natural sedimentation with the aim to improve ion transport and ionic accessibility. The results obtained showed improved cyclability, rate performance, and increased capacitance from 145 to 351 mAh/g. Intercalants like DMSO, urea, and hydrazine is also used to tackle this challenge [108]. Hydrazine monohydrate dissolved in N, N – dimethylformamide is the most used intercalant and is proved to increase interlayer spacing from 7.2 to 10.4 Å. In yet another work, interlayer distance was maintained by a combination of pillared effect of sodium ions and swollen effect of penetration of solvent molecule [109]. Agglomeration of MXene layers during synthesis was found to decrease by synthesis of MXene-holey graphene composite film and gave volumetric capacitance of 1445 F/cm³ [110]. In this way, structuring of MXene enhances conductivity and stability of the device. Restacking can also be prevented by modifying the method of synthesis of MXene as demonstrated by Zahra et al. [111]. V₂CT_x MXene electrodes were fabricated via cation-assisted self-assembly method. During self-assembly process, monovalent alkali cations including Li⁺, Na⁺, and K⁺ were introduced amid MXene sheets, resulting in formation of pillared structures that expands interlayer spacing. Increased accessibility of electrolyte ions aided in enhancing capacitance and rate capability. However, ensuring uniform cation intercalation can turn out to be challenge when extended for practical applications.

Inadequate understanding about effect of surface termination group on different properties of MXene material is another confrontation faced [106]. Removal of -F and -OH functional groups often affect transportation of electrolyte ions and decrease energy storing capability [112]. Developing MXene foam using MgO as hard template was found

to give a capacitance of 203 F/g and a capacitance of 1033 mF/cm³ was obtained by coating Ti₃C₂T_x MXene on activated carbon cloth. Effectively manipulating the functional groups by cation intercalation or tuning synthesis properties proves helpful here.

Oxidation of synthesised MXene results in conversion of highly crystalline MXene to transition metal oxides and amorphous carbon degrading performance of the device fabricated [106]. This can affect the stability as well as overall performance of the MXene [113]. Theoretical studies have shown that oxidation of MXene starts by adsorption of O₂ on Ti surface that causes distortion of Ti layers as well as subsequent fracture of Ti-C bonds. In general, the factors that influence oxidation of MXene includes exposure to light and temperature, conditions of etching, surface terminations, exposure to water or moisture, pH, and flake size of the MXene. Also, harsh etching process forms defects on the surface and edge of MXene which causes degradation in water and oxygen [114]. Inert gases can be used to prevent this danger and thus storing synthesised MXenes in argon sealed containers as well as purging nitrogen gas during synthesis is effective. Etching conditions too can be optimized to reduce defect and active site formation. It is important to preserve MXene materials in a controlled environment minimising exposure to air and moisture. MXene based composites also helps as the composite material can act as a protective layer and reduce the surface area that is exposed to oxidizing agents. In MXene-based nanocomposites, the nanocomposite matrix often creates a barrier effect, limiting its exposure to external agents that favours oxidation. It has been observed that storing MXene in organic solvents will prevent its contact with water and in turn inhibits oxidation. But, the limitation observed here is that MXene do not form a stable suspension when dispersed in organic solvent [113]. Antioxidants like citric acid, ascorbic acid, etc. deters the process of oxidation by acting as protective agent. Dispersing MXene in antioxidants can thus be a solution to the challenge mentioned above. MXene encapsulation involves formation of a uniform layer on the surface of MXene that prevents its exposure to oxygen and water or moisture. Carbon nanoplasting, that hinders surface oxidation and degradation in structure of MXene, is an example to this.

Zhang and Pang [115] evaluated the performance of SC by assessing various parameters, observed the low energy density possessed by them and also concluded that careful optimization is required to balance between energy density, power density, and time constant. The commercial development of the material is constrained by few factors including challenges in the synthesis of MXene material [106]. Use of hazardous hydrofluoric acid and availability along with cost of precursor MAX powders remain limiting factors. It is thus important to develop synthesis methods that limits the use of hazardous chemicals. To develop efficient electrode materials with increased specific surface area and operation window is also a challenge [102]. Often colloidal MXenes are

produced by long mixing or shaking which are not desirable for commercialization of the material [106]. Lowering high cost of production of MXene is substantial for optimizing their use in industrial applications.

8. Machine learning (ML) for prediction of SC performance

Numerous factors influence a supercapacitor's electrochemical performance and understanding how they relate to one another is crucial for figuring out how to increase the supercapacitor's efficiency [116]. Researchers can find hidden patterns and correlations between material properties, design configurations, and performance metrics by using ML to analyze complex datasets. ML-driven techniques greatly speed up the development of supercapacitor technology by enabling predictive modeling, electrode material optimization, and the identification of optimal electrolyte combinations. In addition to making it easier to create high-performance supercapacitors, this ML integration offers practical advice for enhancing cyclic stability, energy density, and power density. Through the analysis of intricate datasets and the discovery of nonlinear relationships between material properties, electrode designs, and electrochemical behavior, ML provides a revolutionary way to overcome these constraints. There are several methods for this, but theories such as the conventional EDL theory are unable to ascertain how surface morphology or pore structures affect the material's capacitance [117].

Important performance metrics like C_{sp} , cyclic stability, and electrical conductivity have been shown to be accurately predicted by ML models, which include algorithms like Random Forest (RF), Artificial Neural Networks (ANN), and Extreme Gradient Boosting (XGBoost). For example, ML has been used to accurately determine how physico-chemical characteristics, like pore size, surface area, and doping levels, affect capacitance. In addition to offering practical insights into ion transport mechanisms that conventional theories are unable to adequately explain, these models allow researchers to optimize electrode materials and electrolyte combinations.

Researchers can produce high-performance supercapacitors more quickly by incorporating ML techniques, which will guarantee improved energy storage options for everything from hybrid electric vehicles to Internet of Things devices.

ML and deep learning (DL), two artificial intelligence technologies, can help with both the design and characterization of MXenes [118]. An integration of first-principles calculation and ML has been used to uncover deeper insights into the complex nature of MXene [119]. Key parameters that are crucial for application in SC like influence of the surface termination group and, stacking of atomic layers were studied. It was observed in the study that O and F terminations were more stable compared to other functional groups. The role of halogen and chalcogen terminations in the stability and functionality of MXene were also explored. It was found that the order of stacking of MXene influence the adsorption properties of MXene. ABA stacking turns out to be more stable than ABC stacking. While DL is excellent at processing complex, high-dimensional datasets like spectral data or microscopy images, ML techniques, like supervised learning, are especially helpful for mapping material properties to performance metrics. As a result, ML algorithms are now used to forecast a supercapacitor's performance based on a variety of input characteristics. The development and optimization of MXene materials for supercapacitor applications can be significantly enhanced by AI and ML [120].

The ability of machine learning models such as Random Forest and XGBoost to handle heterogeneous datasets and provide feature importance rankings—which aid in identifying important structural parameters influencing electrochemical behavior—has led to their widespread adoption. By facilitating data-driven discovery and optimization of cutting-edge materials like MXenes for supercapacitors, artificial intelligence (AI) technologies like ML and DL are transforming materials science. In order to predict electrochemical properties (capacitance,

cycle life) from structural descriptors (interlayer spacing, termination groups), machine learning algorithms (e.g., Random Forest, XGBoost) use feature engineering and supervised learning. For example, XGBoost maximizes predictive performance through gradient boosting, while Random Forest creates an ensemble of decision trees to minimize overfitting. These algorithms are perfect for materials informatics.

These capabilities are expanded by deep learning techniques, especially Convolutional Neural Networks (CNNs) and Graph Neural Networks (GNNs), which automatically extract hierarchical features from raw data, like atomic coordinates or microscopy images. By using hierarchical feature extraction to process high-dimensional data (spectroscopic images, DFT simulations), DL architectures (CNNs, GNNs) further improve predictive accuracy. While techniques like SHAP analysis offer interpretability for mechanistic insights, these AI methods speed up materials design by identifying non-linear structure-property relationships and optimizing synthesis parameters beyond empirical trial-and-error approaches. SHAP (SHapley Additive exPlanations) values, for example, quantify the contribution of each input feature to the model's predictions, offering insights into which MXene properties most significantly impact performance.

The combination of AI with multiscale simulations and automated experimentation enables closed-loop optimization, where ML models suggest new compositions and synthesis conditions for experimental validation. The integration of AI with multiscale modeling and automated experimentation is paving the way for autonomous discovery of next-generation energy storage materials. ML has improved performance prediction in MXene-based supercapacitors by integrating several varied physic-chemical features or electrochemical measurements. Specifically, it is reported that a machine learning model can accurately predict C_{sp} based on the atomic percent of doped elements, electrode configuration, pore characteristics, and parameters set for electrochemical tests [121–123].

Recent advances in explainable AI (XAI) ensure that these models are not just black boxes but provide actionable insights for materials scientists. It helps to predict the properties of MXene skin-like electrodes for enhanced performance forecasts; ML moots a means of understanding and optimizing MXene-based supercapacitors with advanced human-machine interactions [124]. Further, ML was exploited to effectively probe the synergistic effects of heteroatom doping on graphene-based supercapacitors and found optimum synthesis conditions that further attest to improved capacitance and retention rates [122]. For example, ML-guided doping strategies have revealed that nitrogen-functionalized MXenes exhibit enhanced pseudocapacitance due to improved charge transfer kinetics.

Beyond prediction, ML is also being used to optimize electrode architectures, such as preventing MXene restacking through computational screening of intercalants. One approach to the design of intercalants, based on 1D π-d conjugated coordination polymers for MXene interlayers, was able to avoid restacking problems and improve electrochemical activity, hence realizing supercapacitor electrodes with excellent rate performance and stability [125]. Such approaches highlight how AI is transitioning from a predictive tool to an active participant in materials design, accelerating the development of high-performance energy storage systems.

This integration of AI into MXene research not only enhances predictive accuracy but also enables a deeper understanding of structure-property relationships, paving the way for next-generation supercapacitors with tailored performance characteristics.

Zhu et al. [126] made use of artificial neuron network (ANN) to predict electrochemical performance or more specifically, capacitance of carbon-based supercapacitors. ANNs are particularly effective for this application because they can model complex non-linear relationships between material properties and performance metrics through their interconnected neuron architecture. Data from more than 300 published works were collected to extract 681 sets of data to train the ANN model and five features were selected to serve as input. Upon analysis, a

comparison of predicted and real capacitance value was plotted where correlation coefficient of 0.91 was obtained ensuring accurate prediction. Artificial neural networks are computational systems that mimic the human brain's functionality through neuron nodes [127].

Similarly, Su et al. [117] employed four ML algorithms namely, linear regression (LR), support vector regression (SVR), multilayer perceptron model (MLP), and regression tree models (RT) to obtain the relation between input features and performance of carbon-based supercapacitors. These algorithms represent a spectrum of approaches from simple linear models (LR) to more complex non-linear methods (SVR, MLP) and decision-based techniques (RT), allowing comprehensive analysis of the data structure. Among the four, MLP and RT gave

best results. One of the most powerful non-parametric modelling techniques, regression trees offer much flexibility when capturing complicated relationships within data without normalization or scaling [128].

The strength of regression trees lies in their ability to automatically identify important features and handle mixed data types, making them ideal for materials science applications where parameters may have different units and scales. In a different work, four different ML algorithms were used to predict capacitance retention of supercapacitor based on features in both material perspective and device perspective through training based on 801 sets of data prepared from 400 research papers [116]. Two ways, capacitance retention value prediction and capacitance retention grade prediction, was adopted for this. Nearly 15

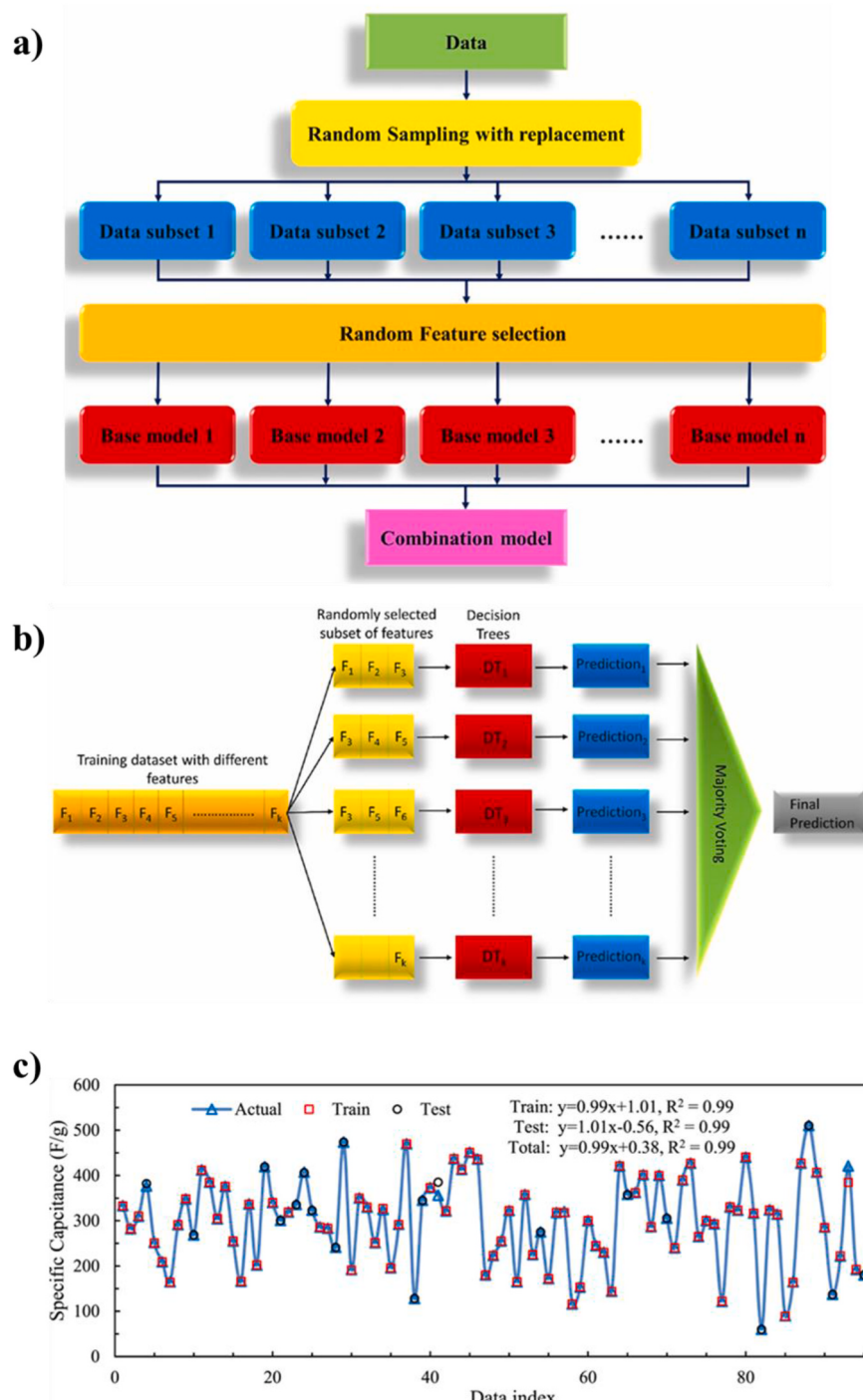


Fig. 8. Model development in a) Random Forest b) Random Subspace [116] c) The actual and predicted values of Csp [135].

attributes acted as input features. The five ML algorithms used for the study included random forest (RF), random committee (RC), random subspace (RS), multiclass classifier (MCC), and random tree (RT) which were then combined to hybrid forms like RF and RC, RS and RF, RC and RF for value prediction model.

Random Forest deserves special attention as it improves prediction accuracy by creating an ensemble of decision trees and aggregating their results, while simultaneously providing feature importance rankings that can guide materials design. The values were categorised into three grades (A, B, and C). A critical analysis on the dependence of capacitance retention on different attributes were done based on obtained correlation from WEKA software. RF is a powerful ensemble learning method mostly applied for large classification and regression tasks; it particularly gained very high predictive accuracy on tabular data, though at the expense of intrinsic complexity, often costing interpretability [129]. Fig. 8(a) represents the model development of RF algorithm. The Random Committee refers to the technique whereby a committee of models is trained on the same dataset and makes the final prediction via some voting process among the trained models [130].

The committee approach reduces variance and minimizes the risk of relying on any single potentially biased model, which is particularly valuable when working with experimental materials data that may contain noise or outliers. In this respect, multi-class classifiers are important in solving complex classification problems involving multiple classes using machine learning techniques [131]. Random Subspace methods lie at the heart of machine learning, offering new solutions in a wide range of domains by selecting random subsets of features to optimize model accuracy and efficiency [132]. Model development of RS is seen in Fig. 8(b). A Random Tree can be considered under different models and constructions that more precisely highlight one or other mechanism at work during its growth and, more generally, its structural properties [133].

Ghosh et al. [134] worked on prediction of performance of cerium oxynitride to be used as electrode for supercapacitor based on ML methods. This study demonstrated how ML can accelerate the screening of novel materials by predicting performance before synthesis, potentially saving significant experimental time and resources. WEKA 3.8.5 software was used to execute ML using data for essential parameters extracted from the existing literature. The parameters used for the study included composition of the material, its morphology, surface area, substrate, potential window, current density, several charge-discharge cycles, and capacitive retention using which a database of metal oxide, nitride, and metal oxynitride was created. In this work too both capacitance grade prediction as well as capacitance value prediction were used for Csp prediction through the algorithms MLP and RF.

The combination of MLP (for capturing complex patterns) and RF (for robust feature selection) created a powerful hybrid approach that leveraged the strengths of both algorithms. Models were studied based on each grade and parameters like false positive rate (FPR), true positive rate (TPR), and area under receiver operating characteristic (AUROC) values were used to select the best model. Mark Hall and Gabi Schmidberger's code was used for principal component analysis (PCA) in order to reduce dimensionality, increase interpretability of data as well as to ensure minimum loss of information. MLP and RF was used to calculate correlation coefficient (R) and mean absolute error (MAE) to predict value of capacitance. Higher R along with lower MAE means a better model. The program predicted cerium oxynitride to be a material of grade 'A' with Csp value close to 200 F/g at 2 A/g. Cyclic stability was examined by adding initial capacitance and number of cycles to the dataset and it was predicted that 90–100 % capacitance would be retained after 10000 cycles. Difference in any synthesis condition can result in change in value of attributes resulting in change in the prediction of value or grade. Predicted values were compared with obtained experimental values. Calculated specific capacity at 2 A/g was close to the value predicted by ML. Also, 50 % capacitance was retained when current density increased by 10 times. The performance of biomass-

based activated carbon electrodes was explored using ANN by Rahimi et al. [135]. 101 data sets from different sources were compiled after an extensive literature review. It was also observed that the actual values as well as predicted values were in agreement with each other as seen in Fig. 8(c). The study emphasize the relevance of optimizing structural features and operational parameters of the material to improve the performance of the SC. Wang et al. [136] used sure independence screening and sparsifying operator (SISSO) algorithm for developing pseudocapacitance formula of MXenes. SISSO is an algorithm that uses sure independence screening principle for feature selection and dimensionality reduction. It narrows down the smallest set of features that predicts target variable and minimizes dataset dimensionality. Incorporation of SISSO in pseudocapacitance research helps in decreasing computational time required. 600 MXenes were explored using ML strategy. It was observed from the study that in case of MXene with group-free surface, pseudocapacitance was regulated by strength of ion adsorption and DOS whereas for surface-functionalized materials, pseudocapacitance is determined by specific heat and electronegativity. These studies manifest how machine learning has huge potential to improve performance prediction and the design of MXene-based supercapacitors for next-generation energy storage. Therefore, applying ML algorithms in material design and optimization will make it possible for researchers to accelerate the discovery of new MXene-based composites most suitable for advanced supercapacitor technologies with superior electrochemical performance.

9. Summary & outlook

MXenes, a novel class of TMCN, has attracted immense interest in research field by their immense potential in SC applications aided by the exceptional electrical conductivity, rich surface functionality, high SSA, and hydrophilicity. In contrast to conventional electrode materials for SC, MXenes exhibit a unique combination of properties that enable better charge storage mechanism in SC. Nevertheless, the electrochemical properties of the material depends on the other factors including interlayer spacing, surface functional groups, and methods of synthesis. This article has reviewed the properties, methods of synthesis, composites and the studies done till date in the above arena. Different method of synthesis, influencing the structural integrity, morphology, and other properties of MXene have been explored. Attempts to enhance supercapacitive performance and to mitigate the limitations of MXenes including self-restacking and oxidation have driven extensive research into DTM MXenes and MXene-based composites. Industrial perspective of MXene-based SCs with a comparative market analysis is also included in the review. A crucial aspect of the review is the integration of ML methods to predict performance of SC. ML algorithms including ANN, RF, RT, RS, and SISSO have been widely used to explore materials for application in energy sector and also analyze datasets and then predict Csp, energy density, capacitance retention and such features with the help of data studied. This has opened new avenues to escalate the development of highly efficient SCs.

To unlock full potential of MXene-based SCs, several challenges need to be addressed. Developing environment-friendly, fluoride-free synthesis methods without compromising the yield or structural integrity that is important for large-scale synthesis must be focused on. Future research should explore methods to overcome restacking and improvising charge transport dynamics of the material. Although, significant progress has been achieved in MXene material for application in SC, further exploration is inevitable to broaden their application scope and optimize their supercapacitive performance. In-depth understanding of the charge storage mechanism of MXenes when subjected to varying operational conditions is also significant for enhancing performance of MXene. Key features like cyclic stability and environmental stability demands focus as it ensures long-term reliability in practical applications. Interweaving ML for accurate prediction of MXene based materials demands collaboration among the computational and experimental

researchers. Addressing these challenges will enable MXenes to revolutionize energy storage industry.

CRediT authorship contribution statement

Daisy Maria Saju: Writing – original draft, Investigation, Conceptualization. **R. Sapna:** Writing – original draft, Conceptualization. **Utpal Deka:** Writing – review & editing, Resources. **K. Hareesh:** Writing – review & editing, Supervision, Resources, Funding acquisition, Conceptualization.

Declaration of competing interest

The authors declare that they have no known competing financial interests or personal relationships that could have appeared to influence the work reported in this paper.

Acknowledgements

DMS acknowledges Manipal Academy of Higher Education for providing Dr. T.M.A. Pai Scholarship.

Data availability

No data was used for the research described in the article.

References

- [1] P. S, N. K, S.M. Jeong, C.S. Rout, MXene–carbon based hybrid materials for supercapacitor applications, *Energy Adv* 3 (2024) 341–365, <https://doi.org/10.1039/D3YA00502J>.
- [2] M. Vangari, T. Pryor, L. Jiang, Supercapacitors: review of materials and fabrication methods, *J. Energy Eng.* 139 (2013) 72–79, [https://doi.org/10.1061/\(ASCE\)EY.1943-7897.0000102](https://doi.org/10.1061/(ASCE)EY.1943-7897.0000102).
- [3] H.A. Khan, M. Tawalbeh, B. Aljawrneh, W. Abuwafat, A. Al-Othman, H. Sadeghifar, A.G. Olabi, A comprehensive review on supercapacitors: their promise to flexibility, high temperature, materials, design, and challenges, *Energy* 295 (2024) 131043, <https://doi.org/10.1016/j.energy.2024.131043>.
- [4] M. Armand, J.-M. Tarascon, Building better batteries, *Nature* 451 (2008) 652–657, <https://doi.org/10.1038/451652a>.
- [5] N.I. Jalal, R.I. Ibrahim, M.K. Oudah, A review on supercapacitors: types and components, *J. Phys.: Conf. Ser.* 1973 (2021) 012015, <https://doi.org/10.1088/1742-6596/1973/1/012015>.
- [6] Q. Zhu, D. Zhao, M. Cheng, J. Zhou, K.A. Owusu, L. Mai, Y. Yu, A new view of supercapacitors: integrated supercapacitors, *Adv. Energy Mater.* 9 (2019) 1901081, <https://doi.org/10.1002/aenm.201901081>.
- [7] Q. Tan, P. Irwin, Y. Cao, Advanced dielectrics for capacitors, *IEEJ Trans.FM* 126 (2006) 1153–1159, <https://doi.org/10.1541/ieejfms.126.1153>.
- [8] J. Sun, B. Luo, H. Li, A review on the conventional capacitors, supercapacitors, and emerging hybrid ion capacitors: past, present, and future, *Adv. Energy Sustain. Res.* 3 (2022) 2100191, <https://doi.org/10.1002/aesr.202100191>.
- [9] Y. Wang, Y. Song, Y. Xia, Electrochemical capacitors: mechanism, materials, systems, characterization and applications, *Chem. Soc. Rev.* 45 (2016) 5925–5950, <https://doi.org/10.1039/C5CS00580A>.
- [10] M.G. Ashritha, K. Hareesh, Electrode materials for EDLC and pseudocapacitors, in: *Smart Supercapacitors*, Elsevier, 2023, pp. 179–198, <https://doi.org/10.1016/B978-0-323-90530-5.00033-2>.
- [11] M.F. Iqbal, F. Nasir, F. Shabbir, Z.U.D. Babar, M.F. Saleem, K. Ullah, N. Sun, F. Ali, Supercapacitors: an emerging energy storage system, *Adv. Energy Sustain. Res.* 2400412, <https://doi.org/10.1002/aesr.202400412>.
- [12] B. Anasori, Y. Xie, M. Beidaghi, J. Lu, B.C. Hosler, L. Hultman, P.R.C. Kent, Y. Gogotsi, M.W. Barsoum, Two-dimensional, ordered, double transition metals carbides (MXenes), *ACS Nano* 9 (2015) 9507–9516, <https://doi.org/10.1021/acsnano.5b03591>.
- [13] Y. Wu, W. Yuan, M. Xu, S. Bai, Y. Chen, Z. Tang, C. Wang, Y. Yang, X. Zhang, Y. Yuan, M. Chen, X. Zhang, B. Liu, L. Jiang, Two-dimensional Black phosphorus: properties, fabrication and application for flexible supercapacitors, *Chem. Eng. J.* 412 (2021) 128744, <https://doi.org/10.1016/j.cej.2021.128744>.
- [14] X. Liu, F. Xu, Z. Li, Z. Liu, W. Yang, Y. Zhang, H. Fan, H.Y. Yang, Design strategy for MXene and metal chalcogenides/oxides hybrids for supercapacitors, secondary batteries and electro/photocatalysis, *Coord. Chem. Rev.* 464 (2022) 214544, <https://doi.org/10.1016/j.ccr.2022.214544>.
- [15] S. Raj Ka, P. Mane, S. Radhakrishnan, B. Chakraborty, C.S. Rout, Heterostructured metallic 1T-VSe₂/Ti₃C₂T_x MXene nanosheets for energy storage, *ACS Appl. Nano Mater.* 5 (2022) 4423–4436, <https://doi.org/10.1021/acsanm.2c00533>.
- [16] U. Shahzad, H.M. Marwani, M. Saeed, A.M. Asiri, M.M. Rahman, Two-dimensional MXenes as emerging materials: a comprehensive review, *ChemistrySelect* 8 (2023) e202300737, <https://doi.org/10.1002/slct.202300737>.
- [17] M. Naguib, M. Kurtoglu, V. Presser, J. Lu, J. Niu, M. Heon, L. Hultman, Y. Gogotsi, M.W. Barsoum, Two-dimensional nanocrystals produced by exfoliation of Ti₃AlC₂, *Adv. Mater.* 23 (2011) 4248–4253, <https://doi.org/10.1002/adma.201102306>.
- [18] K. Deshmukh, T. Kovářík, S.K. Khadheer Pasha, State of the art recent progress in two dimensional MXenes based gas sensors and biosensors: a comprehensive review, *Coord. Chem. Rev.* 424 (2020) 213514, <https://doi.org/10.1016/j.ccr.2020.213514>.
- [19] B. Anasori, M. Dahlqvist, J. Halim, E.J. Moon, J. Lu, B.C. Hosler, E.N. Caspi, S. J. May, L. Hultman, P. Eklund, J. Rosén, M.W. Barsoum, Experimental and theoretical characterization of ordered MAX phases Mo₂TiAlC₂ and Mo₂Ti₂AlC₃, *J. Appl. Phys.* 118 (2015) 094304, <https://doi.org/10.1063/1.4929640>.
- [20] M. Alhabeb, K. Maleski, B. Anasori, P. Lelyukh, L. Clark, S. Sin, Y. Gogotsi, Guidelines for synthesis and processing of two-dimensional titanium carbide (Ti₃C₂T_x MXene), *Chem. Mater.* 29 (2017) 7633–7644, <https://doi.org/10.1021/acs.chemmater.7b02847>.
- [21] S.K. Kailasa, D.J. Joshi, J.R. Koduru, N.I. Malek, Review on MXenes-based nanomaterials for sustainable opportunities in energy storage, sensing and electrocatalytic reactions, *J. Mol. Liq.* 342 (2021) 117524, <https://doi.org/10.1016/j.molliq.2021.117524>.
- [22] C. Xu, L. Wang, Z. Liu, L. Chen, J. Guo, N. Kang, X.-L. Ma, H.-M. Cheng, W. Ren, Large-area high-quality 2D ultrathin Mo₂C superconducting crystals, *Nat. Mater.* 14 (2015) 1135–1141, <https://doi.org/10.1038/nmat4374>.
- [23] M. Gao, F. Wang, S. Yang, A. Gaetano Ricciardulli, F. Yu, J. Li, J. Sun, R. Wang, Y. Huang, P. Zhang, X. Lu, Engineered 2D MXene-based materials for advanced supercapacitors and micro-supercapacitors, *Mater. Today* 72 (2024) 318–358, <https://doi.org/10.1016/j.matto.2023.12.009>.
- [24] X.-H. Zha, K. Luo, Q. Li, Q. Huang, J. He, X. Wen, S. Du, Role of the surface effect on the structural, electronic and mechanical properties of the carbide MXenes, *EPL* 111 (2015) 26007, <https://doi.org/10.1209/0295-5075/111/26007>.
- [25] M.P. Bilibana, Electrochemical properties of MXenes and applications, *Advanced Sensor and Energy Materials* 2 (2023) 100080, <https://doi.org/10.1016/j.asesm.2023.100080>.
- [26] S. Karamat, M. Kashif, S. Anwar, U. Batool, M. Talha, U. Khalique, M.M. Rahman, Unveiling the latest advancements in vanadium carbide MXene based supercapacitors and their future trends, *Chem. Asian J.* 19 (2024) e202300919, <https://doi.org/10.1002/asia.202300919>.
- [27] K. Maleski, C.E. Ren, M.-Q. Zhao, B. Anasori, Y. Gogotsi, Size-dependent physical and electrochemical properties of two-dimensional MXene flakes, *ACS Appl. Mater. Interfaces* 10 (2018) 24491–24498, <https://doi.org/10.1021/acsami.8b04662>.
- [28] B. Akgenç, Intriguing of two-dimensional janus surface-functionalized MXenes: an ab initio calculation, *Comput. Mater. Sci.* 171 (2020) 109231, <https://doi.org/10.1016/j.commatsci.2019.109231>.
- [29] B. Anasori, C. Shi, E.J. Moon, Y. Xie, C.A. Voigt, P.R.C. Kent, S.J. May, S.J. L. Billinge, M.W. Barsoum, Y. Gogotsi, Control of electronic properties of 2D carbides (MXenes) by manipulating their transition metal layers, *Nanoscale Horiz* 1 (2016) 227–234, <https://doi.org/10.1039/C5NH00125K>.
- [30] L. Hong, R.F. Klie, S. Öğüt, First-principles study of size- and edge-dependent properties of MXene nanoribbons, *Phys. Rev. B* 93 (2016) 115412, <https://doi.org/10.1103/PhysRevB.93.115412>.
- [31] Y. Zhou, G. Zhai, T. Yan, J.S. Francisco, H. Tian, Q. Huang, S. Du, Effects of different surface functionalization and doping on the electronic transport properties of M₂CT_x–M₂CO₂ heterojunction devices, *J. Phys. Chem. C* 122 (2018) 14908–14917, <https://doi.org/10.1021/acs.jpcc.8b02026>.
- [32] A. Miranda, J. Halim, M.W. Barsoum, A. Lorke, Electronic properties of freestanding Ti₃C₂T_x MXene monolayers, *Appl. Phys. Lett.* 108 (2016) 033102, <https://doi.org/10.1063/1.4939971>.
- [33] M. Mariano, O. Mashtalar, F.Q. Antonio, W.-H. Ryu, B. Deng, F. Xia, Y. Gogotsi, A. D. Taylor, Solution-processed titanium carbide MXene films examined as highly transparent conductors, *Nanoscale* 8 (2016) 16371–16378, <https://doi.org/10.1039/C6NR03682A>.
- [34] Y. Wu, X. Li, H. Zhao, F. Yao, J. Cao, Z. Chen, X. Huang, D. Wang, Q. Yang, Recent advances in transition metal carbides and nitrides (MXenes): characteristics, environmental remediation and challenges, *Chem. Eng. J.* 418 (2021) 129296, <https://doi.org/10.1016/j.cej.2021.129296>.
- [35] R.A. Soomro, P. Zhang, B. Fan, Y. Wei, B. Xu, Progression in the oxidation stability of MXenes, *Nano-Micro Lett.* 15 (108) (2023), <https://doi.org/10.1007/s40820-023-01069-7>.
- [36] B. Xia, Z. Wang, T. Wang, S. Chen, H. Wu, B. Zhang, Y. Si, Z. Chen, B.-W. Li, Z. Kou, D. He, Bridging sheet size controls densification of MXene films for robust electromagnetic interference shielding, *iScience* 25 (2022) 105001, <https://doi.org/10.1016/j.isci.2022.105001>.
- [37] X. Zhao, A. Vashisth, E. Prehn, W. Sun, S.A. Shah, T. Habib, Y. Chen, Z. Tan, J. L. Lutkenhaus, M. Radovic, M.J. Green, Antioxidants unlock shelf-stable Ti₃C₂T_x (MXene) nanosheet dispersions, *Matter* 1 (2019) 513–526, <https://doi.org/10.1016/j.matt.2019.05.020>.
- [38] V. Natu, J.L. Hart, M. Sokol, H. Chiang, M.L. Taheri, M.W. Barsoum, Edge capping of 2D-MXene sheets with polyanionic salts to mitigate oxidation in aqueous colloidal suspensions, *Angew. Chem. Int. Ed.* 58 (2019) 12655–12660, <https://doi.org/10.1002/anie.201906138>.

- [39] M. Naguib, O. Mashtalir, J. Carle, V. Presser, J. Lu, L. Hultman, Y. Gogotsi, M. W. Barsoum, Two-dimensional transition metal carbides, *ACS Nano* 6 (2012) 1322–1331, <https://doi.org/10.1021/nm204153h>.
- [40] Y. Ying, Y. Liu, X. Wang, Y. Mao, W. Cao, P. Hu, X. Peng, Two-dimensional titanium carbide for efficiently reductive removal of highly toxic Chromium(VI) from water, *ACS Appl. Mater. Interfaces* 7 (2015) 1795–1803, <https://doi.org/10.1021/am507472z>.
- [41] Y. Wei, P. Zhang, R.A. Soomro, Q. Zhu, B. Xu, Advances in the synthesis of 2D MXenes, *Adv. Mater.* 33 (2021) 2103148, <https://doi.org/10.1002/adma.202103148>.
- [42] M. Anayee, N. Kurra, M. Alhabeb, M. Seredych, M.N. Hedhili, A.-H. Emwas, H. N. Alshareef, B. Anasori, Y. Gogotsi, Role of acid mixtures etching on the surface chemistry and sodium ion storage in $Ti_3C_2T_x$ MXene, *Chem. Commun.* 56 (2020) 6090–6093, <https://doi.org/10.1039/D0CC01042A>.
- [43] M. Alhabeb, K. Maleski, T.S. Mathis, A. Sarycheva, C.B. Hatter, S. Uzun, A. Levitt, Y. Gogotsi, Selective etching of silicon from Ti_3SiC_2 (MAX) to obtain 2D titanium carbide (MXene), *Angew. Chem. Int. Ed.* 57 (2018) 5444–5448, <https://doi.org/10.1002/anie.201802232>.
- [44] W. Sun, S.A. Shah, Y. Chen, Z. Tan, H. Gao, T. Habib, M. Radovic, M.J. Green, Electrochemical etching of Ti_2AlC to Ti_2CT_x (MXene) in low-concentration hydrochloric acid solution, *J. Mater. Chem. A* 5 (2017) 21663–21668, <https://doi.org/10.1039/C7TA05574A>.
- [45] S. Yang, P. Zhang, F. Wang, A.G. Ricciardulli, M.R. Lohe, P.W.M. Blom, X. Feng, Fluoride-Free synthesis of two-dimensional titanium carbide (MXene) using A binary aqueous system, *Angew. Chem. Int. Ed.* 57 (2018) 15491–15495, <https://doi.org/10.1002/anie.201809662>.
- [46] M. Ghidru, M.R. Lukatskaya, M.-Q. Zhao, Y. Gogotsi, M.W. Barsoum, Conductive two-dimensional titanium carbide ‘clay’ with high volumetric capacitance, *Nature* 516 (2014) 78–81, <https://doi.org/10.1038/nature13970>.
- [47] J. Wu, Y. Wang, Y. Zhang, H. Meng, Y. Xu, Y. Han, Z. Wang, Y. Dong, X. Zhang, Highly safe and ionothermal synthesis of Ti_3C_2 MXene with expanded interlayer spacing for enhanced lithium storage, *J. Energy Chem.* 47 (2020) 203–209, <https://doi.org/10.1016/j.jecchem.2019.11.029>.
- [48] J. Halim, M.R. Lukatskaya, K.M. Cook, J. Lu, C.R. Smith, L.-Å. Näslund, S.J. May, L. Hultman, Y. Gogotsi, P. Eklund, M.W. Barsoum, Transparent conductive two-dimensional titanium carbide epitaxial thin films, *Chem. Mater.* 26 (2014) 2374–2381, <https://doi.org/10.1021/cm500641a>.
- [49] Y. Li, H. Shao, Z. Lin, J. Lu, L. Liu, B. Dupoyer, P.O.Å. Persson, P. Eklund, L. Hultman, M. Li, K. Chen, X.-H. Zha, S. Du, P. Rozier, Z. Chai, E. Raymundo-Piñero, P.-L. Taberna, P. Simon, Q. Huang, A general lewis acidic etching route for preparing MXenes with enhanced electrochemical performance in non-aqueous electrolyte, *Nat. Mater.* 19 (2020) 894–899, <https://doi.org/10.1038/s41563-020-0657-0>.
- [50] P. Urbankowski, B. Anasori, T. Makaryan, D. Er, S. Kota, P.L. Walsh, M. Zhao, V. B. Shenoy, M.W. Barsoum, Y. Gogotsi, Synthesis of two-dimensional titanium nitride Ti_4N_3 (MXene), *Nanoscale* 8 (2016) 11385–11391, <https://doi.org/10.1039/C6NR02253G>.
- [51] X. Xie, Y. Xue, L. Li, S. Chen, Y. Nie, W. Ding, Z. Wei, Surface Al leached Ti_3AlC_2 as a substitute for carbon for use as a catalyst support in a harsh corrosive electrochemical system, *Nanoscale* 6 (2014) 11035–11040, <https://doi.org/10.1039/C4NR02080D>.
- [52] C. Peng, P. Wei, X. Chen, Y. Zhang, F. Zhu, Y. Cao, H. Wang, H. Yu, F. Peng, A hydrothermal etching route to synthesis of 2D MXene (Ti_3C_2 , Nb_2C): enhanced exfoliation and improved adsorption performance, *Ceram. Int.* 44 (2018) 18886–18893, <https://doi.org/10.1016/j.ceramint.2018.07.124>.
- [53] L. Wang, H. Zhang, B. Wang, C. Shen, C. Zhang, Q. Hu, A. Zhou, B. Liu, Synthesis and electrochemical performance of Ti_3C_2Tx with hydrothermal process, *electron*, *Mater. Lett.* 12 (2016) 702–710, <https://doi.org/10.1007/s13391-016-6088-z>.
- [54] Z. Li, L. Wang, D. Sun, Y. Zhang, B. Liu, Q. Hu, A. Zhou, Synthesis and thermal stability of two-dimensional carbide MXene Ti_3C_2 , *Mater. Sci. Eng., B* 191 (2015) 33–40, <https://doi.org/10.1016/j.mseb.2014.10.009>.
- [55] Z. Wang, V. Kochat, P. Pandey, S. Kashyap, S. Chattopadhyay, A. Samanta, S. Sarkar, P. Manimunda, X. Zhang, S. Asif, A.K. Singh, K. Chattopadhyay, C. S. Tiwary, P.M. Ajayan, Metal immiscibility route to synthesis of ultrathin carbides, borides, and nitrides, *Adv. Mater.* 29 (2017) 1700364, <https://doi.org/10.1002/adma.201700364>.
- [56] Y. Cheng, W. Lyu, Z. Wang, H. Ouyang, A. Zhang, J. Sun, T. Yang, B. Fu, B. He, MXenes: synthesis, incorporation, and applications in ultrafast lasers, *Nanotechnology* 32 (2021) 392003, <https://doi.org/10.1088/1361-6528/ac0d7e>.
- [57] F. Zhang, Z. Zhang, H. Wang, C.H. Chan, N.Y. Chan, X.X. Chen, J.-Y. Dai, Plasma-enhanced pulsed-laser deposition of single-crystalline M o 2 C ultrathin superconducting films, *Phys. Rev. Mater.* 1 (2017) 034002, <https://doi.org/10.1103/PhysRevMaterials.1.034002>.
- [58] P. Yan, R. Zhang, J. Jia, C. Wu, A. Zhou, J. Xu, X. Zhang, Enhanced supercapacitive performance of delaminated two-dimensional titanium carbide/carbon nanotube composites in alkaline electrolyte, *J. Power Sources* 284 (2015) 38–43, <https://doi.org/10.1016/j.jpowsour.2015.03.017>.
- [59] R.A. Murugesan, K.C. Nagamuthu Raja, Capacitance performance of Ti_3C_2Tx MXene nanosheets on alkaline and neutral electrolytes, *Mater. Res. Bull.* 163 (2023) 112217, <https://doi.org/10.1016/j.materresbull.2023.112217>.
- [60] R.B. Rakhi, B. Ahmed, M.N. Hedhili, D.H. Anjum, H.N. Alshareef, Effect of postetch annealing gas composition on the structural and electrochemical properties of Ti_2CT_x MXene electrodes for supercapacitor applications, *Chem. Mater.* 27 (2015) 5314–5323, <https://doi.org/10.1021/acs.chemmater.5b01623>.
- [61] Q.X. Xia, N.M. Shinde, T. Zhang, J.M. Yun, A. Zhou, R.S. Mane, S. Mathur, K. H. Kim, Seawater electrolyte-mediated high volumetric MXene-based electrochemical symmetric supercapacitors, *Dalton Trans.* 47 (2018) 8676–8682, <https://doi.org/10.1039/C8DT01375F>.
- [62] S.A. Melchior, K. Raju, I.S. Ike, R.M. Erasmus, G. Kabongo, I. Sigalas, S.E. Iyuke, K.I. Ozoemena, High-voltage symmetric supercapacitor based on 2D titanium carbide (MXene, Ti_2CT_x)/Carbon nanosphere composites in a neutral aqueous electrolyte, *J. Electrochem. Soc.* 165 (2018) A501–A511, <https://doi.org/10.1149/2.0401803jes>.
- [63] Q. Wang, Z. Zhang, Z. Zhang, X. Zhou, G. Ma, Facile synthesis of MXene/MnO₂ composite with high csp, *J. Solid State Electrochem.* 23 (2019) 361–365, <https://doi.org/10.1007/s10008-018-4143-4>.
- [64] Q. Fu, X. Wang, N. Zhang, J. Wen, L. Li, H. Gao, X. Zhang, Self-assembled Ti_3C_2Tx /SCNT composite electrode with improved electrochemical performance for supercapacitor, *J. Colloid Interface Sci.* 511 (2018) 128–134, <https://doi.org/10.1016/j.jcis.2017.09.104>.
- [65] L. Yang, W. Zheng, P. Zhang, J. Chen, W.B. Tian, Y.M. Zhang, Z.M. Sun, MXene/CNTs films prepared by electrophoretic deposition for supercapacitor electrodes, *J. Electroanal. Chem.* (2018) 1–6, <https://doi.org/10.1016/j.jelechem.2018.10.024>, 830–831.
- [66] R. N, K. A, M.H. M, N.M. R, D. Mondal, S.K. Nataraj, D. Ghosh, Binder free self-standing high performance supercapacitive electrode based on graphene/titanium carbide composite aerogel, *Appl. Surf. Sci.* 481 (2019) 892–899, <https://doi.org/10.1016/j.apsusc.2019.03.086>.
- [67] Z. Wang, S. Qin, S. Seyedin, J. Zhang, J. Wang, A. Levitt, N. Li, C. Haines, R. Ovalle-Robles, W. Lei, Y. Gogotsi, R.H. Baughman, J.M. Razal, High-performance biskrolled MXene/Carbon nanotube yarn supercapacitors, *Small* 14 (2018) 1802225, <https://doi.org/10.1002/smll.201802225>.
- [68] T. Zheng, X. Zhang, Y. Li, Y. Zhu, W. Yan, Z. Zhao, L. Zhang, C. Bai, X. Wang, Wet-spinning of continuous hyaluronic-based MXene/CNTs hybrid fibers for flexible supercapacitor applications, *Mater. Lett.* 336 (2023) 133891, <https://doi.org/10.1016/j.matlet.2023.133891>.
- [69] K. Nasrin, M. Arunkumar, N. Koushik Kumar, V. Sudharshan, S. Rajasekar, D. Mukhilan, M. Arshad, M. Sathish, A rationally designed hetero-assembly of 2D/2D Nitrogen-doped MXene/Graphene via supercritical fluid processing for high energy durable supercapacitors, *Chem. Eng. J.* 474 (2023) 145505, <https://doi.org/10.1016/j.cej.2023.145505>.
- [70] H. Li, Y. Hou, F. Wang, X. Zhuang, L. Niu, X. Feng, Flexible all-solid-state supercapacitors with high volumetric capacitances boosted by solution processable MXene and electrochemically exfoliated graphene, *Adv. Energy Mater.* 7 (2017) 1601847, <https://doi.org/10.1002/aenm.201601847>.
- [71] J. Yang, W. Bao, P. Jaumaux, S. Zhang, C. Wang, G. Wang, MXene-Based composites: synthesis and applications in rechargeable batteries and supercapacitors, *Adv. Mater. Interfac.* 6 (2019) 1802004, <https://doi.org/10.1002/admi.201802004>.
- [72] Y. Tang, J. Zhu, C. Yang, F. Wang, Enhanced supercapacitive performance of Manganese oxides doped two-dimensional titanium carbide nanocomposite in alkaline electrolyte, *J. Alloys Compd.* 685 (2016) 194–201, <https://doi.org/10.1016/j.jallcom.2016.05.221>.
- [73] W. Wang, G. Chen, W. Kong, J. Chen, L. Pu, J. Gong, H. Zhang, Y. Dai, Sandwich-like high-performance Ti_3C_2Tx MXene/NiCo2O4 nanosphere composites for asymmetric supercapacitor application, *J. Energy Storage* 86 (2024) 111097, <https://doi.org/10.1016/j.est.2024.111097>.
- [74] Lu Wang, Jiayao Cao, Ying-Hua Zhou, Xiaoheng Liu, Design and characterization of monolayer Ti_3C_2 MXene/NiCo2O4 nanocones hybrid architecture for asymmetric supercapacitors. <https://doi.org/10.1016/j.jelechem.2022.116787>, 2022.
- [75] J. Guo, Y. Zhao, A. Liu, T. Ma, Electrostatic self-assembly of 2D delaminated MXene (Ti_3C_2) onto Ni foam with superior electrochemical performance for supercapacitor, *Electrochim. Acta* 305 (2019) 164–174, <https://doi.org/10.1016/j.electacta.2019.03.025>.
- [76] S.T. E, D.T. Tran, S. Jena, Y. Bai, S. Prabhakaran, D.H. Kim, N.H. Kim, J.H. Lee, Flexible 2D borophene-stacked MXene heterostructure for high-performance supercapacitors, *Chem. Eng. J.* 481 (2024) 148266, <https://doi.org/10.1016/j.cej.2023.148266>.
- [77] J. Li, X. Tian, K. He, S. Gao, Z. Wu, S. Yang, F. Wang, A.G. Ricciardulli, S. Wang, Y. Gao, P. Zhang, X. Lu, 0D–1D–2D multidimensional heterostructure films for high-performance flexible microsupercapacitors, *ACS Appl. Mater. Interfaces* 16 (2024) 67706–67714, <https://doi.org/10.1021/acsami.4c13973>.
- [78] P. Sun, J. Liu, Q. Liu, J. Yu, R. Chen, J. Zhu, G. Sun, Y. Li, P. Liu, J. Wang, An inkjet-printing ink based on porous NiS/N-MXene for high-performance asymmetric micro-supercapacitors and self-powered microelectronics, *Chem. Eng. J.* 474 (2023) 145466, <https://doi.org/10.1016/j.cej.2023.145466>.
- [79] Z. Liu, L. Zheng, L. Sun, Y. Qian, J. Wang, M. Li, Cr_{2/3}Ti_{1/3}₂AlC₂ and (Cr_{5/8}Ti_{3/8})₄AlC₃: new MAX -phase compounds in Ti – cr – al – c System, *J. Am. Ceram. Soc.* 97 (2014) 67–69, <https://doi.org/10.1111/jace.12731>.
- [80] I. Hussain, U. Sajjad, O.J. Kewate, U. Amara, F. Bibi, A. Hanan, D. Potphode, M. Ahmad, M.S. Javed, P. Rosaiah, S. Hussain, K. Khan, Z. Ajmal, S. Punniyakoti, S.S. Alarfaji, J.-H. Kang, W. Al Zoubi, S. Sahoo, K. Zhang, Double transition-metal MXenes: classification, properties, machine learning, artificial intelligence, and energy storage applications, *Materials Today Physics* 42 (2024) 101382, <https://doi.org/10.1016/j.mtphys.2024.101382>.
- [81] M.M. Baig, I.H. Gul, S.M. Baig, F. Shahzad, 2D MXenes: synthesis, properties, and electrochemical energy storage for supercapacitors – a review, *J. Electroanal. Chem.* 904 (2022) 115920, <https://doi.org/10.1016/j.jelechem.2021.115920>.

- [82] R. Jayan, A. Vashisth, M.M. Islam, First-principles investigation of elastic and electronic properties of double transition metal carbide MXenes, *J. Am. Ceram. Soc.* 105 (2022) 4400–4413, <https://doi.org/10.1111/jace.18394>.
- [83] Z. Hao, S. Zhang, S. Yang, X. Li, Y. Gao, J. Peng, L. Li, L. Bao, X. Li, Bridged Ti₃C₂T_x MXene film with superior oxidation resistance and structural stability for high-performance flexible supercapacitors, *ACS Appl. Energy Mater.* 5 (2022) 2898–2908, <https://doi.org/10.1021/acsaelm.1c03575>.
- [84] Z. Du, C. Wu, Y. Chen, Z. Cao, R. Hu, Y. Zhang, J. Gu, Y. Cui, H. Chen, Y. Shi, J. Shang, B. Li, S. Yang, High-Entropy atomic layers of transition-metal carbides (MXenes), *Adv. Mater.* 33 (2021) 2101473, <https://doi.org/10.1002/adma.202101473>.
- [85] F. Bibi, A. Numan, Y.S. Tan, M. Khalid, Facile extraction of Mo₂Ti₂C₃T_x MXene via hydrothermal synthesis for electrochemical energy storage, *J. Energy Storage* 85 (2024) 111154, <https://doi.org/10.1016/j.est.2024.111154>.
- [86] H. Zhou, Y. Lu, F. Wu, L. Fang, H. Luo, Y. Zhang, M. Zhou, MnO₂ nanorods/MXene/CC composite electrode for flexible supercapacitors with enhanced electrochemical performance, *J. Alloys Compd.* 802 (2019) 259–268, <https://doi.org/10.1016/j.jallcom.2019.06.173>.
- [87] Y. Zhou, K. Maleski, B. Anasori, J.O. Thostenson, Y. Pang, Y. Feng, K. Zeng, C. B. Parker, S. Zauscher, Y. Gogotsi, J.T. Glass, C. Cao, Ti₃C₂T_x MXene-Reduced graphene oxide composite electrodes for stretchable supercapacitors, *ACS Nano* 14 (2020) 3576–3586, <https://doi.org/10.1021/acsnano.9b10066>.
- [88] Y. Ren, J. Zhu, L. Wang, H. Liu, Y. Liu, W. Wu, F. Wang, Synthesis of polyaniline nanoparticles deposited on two-dimensional titanium carbide for high-performance supercapacitors, *Mater. Lett.* 214 (2018) 84–87, <https://doi.org/10.1016/j.matlet.2017.11.060>.
- [89] C. John Zhang, B. Anasori, A. Seral-Ascaso, S. Park, N. McEvoy, A. Shmeliov, G. S. Duesberg, J.N. Coleman, Y. Gogotsi, V. Nicolosi, Transparent, flexible, and conductive 2D titanium carbide (MXene) films with high volumetric capacitance, *Adv. Mater.* 29 (2017) 1702678, <https://doi.org/10.1002/adma.201702678>.
- [90] L. Shen, X. Zhou, X. Zhang, Y. Zhang, Y. Liu, W. Wang, W. Si, X. Dong, Carbon-intercalated Ti₃C₂T_x MXene for high-performance electrochemical energy storage, *J. Mater. Chem. A* 6 (2018) 23513–23520, <https://doi.org/10.1039/C8TA09600G>.
- [91] C. Yang, Y. Tang, Y. Tian, Y. Luo, M. Faraz Ud Din, X. Yin, W. Que, Flexible nitrogen-doped 2D titanium carbides (MXene) films constructed by an Ex situ solvothermal method with extraordinary volumetric capacitance, *Adv. Energy Mater.* 8 (2018) 1802087, <https://doi.org/10.1002/aenm.201802087>.
- [92] J. Yan, C.E. Ren, K. Maleski, C.B. Hatter, B. Anasori, P. Urbankowski, A. Sarycheva, Y. Gogotsi, Flexible MXene/Graphene films for ultrafast supercapacitors with outstanding volumetric capacitance, *Adv. Funct. Mater.* 27 (2017) 1701264, <https://doi.org/10.1002/adfm.201701264>.
- [93] Y. Wang, J. Sun, X. Qian, Y. Zhang, L. Yu, R. Niu, H. Zhao, J. Zhu, 2D/2D heterostructures of nickel molybdate and MXene with strong coupled synergistic effect towards enhanced supercapacitor performance, *J. Power Sources* 414 (2019) 540–546, <https://doi.org/10.1016/j.jpowsour.2019.01.036>.
- [94] S. Kumar, M.A. Rehman, S. Lee, M. Kim, H. Hong, J.-Y. Park, Y. Seo, Supercapacitors based on Ti₃C₂T_x MXene extracted from supernatant and current collectors passivated by CVD-Graphene, *Sci. Rep.* 11 (2021) 649, <https://doi.org/10.1038/s41598-020-80799-9>.
- [95] X. Wang, H. Li, H. Li, S. Lin, W. Ding, X. Zhu, Z. Sheng, H. Wang, X. Zhu, Y. Sun, 2D/2D 1T-MoS₂/Ti₃C₂ MXene heterostructure with excellent supercapacitor performance, *Adv. Funct. Mater.* 30 (2020) 0190302, <https://doi.org/10.1002/adfm.201910302>.
- [96] J. Zhao, A.F. Burke, Review on supercapacitors: technologies and performance evaluation, *J. Energy Chem.* 59 (2021) 276–291, <https://doi.org/10.1016/j.jecchem.2020.11.013>.
- [97] X. Zhang, Z. Zhang, H. Pan, W. Salman, Y. Yuan, Y. Liu, A portable high-efficiency electromagnetic energy harvesting system using supercapacitors for renewable energy applications in railroads, *Energy Convers. Manag.* 118 (2016) 287–294, <https://doi.org/10.1016/j.enconman.2016.04.012>.
- [98] F. Wang, C. Jiang, C. Tang, S. Bi, Q. Wang, D. Du, J. Song, High output nano-energy cell with piezoelectric nanogenerator and porous supercapacitor dual functions – a technique to provide sustaining power by harvesting intermittent mechanical energy from surroundings, *Nano Energy* 21 (2016) 209–216, <https://doi.org/10.1016/j.nanoen.2016.01.018>.
- [99] J. Kindracki, P. Paszkiewicz, Ł. Mężyk, Resistojet thruster with supercapacitor power source – design and experimental research, *Aero. Sci. Technol.* 92 (2019) 847–857, <https://doi.org/10.1016/j.ast.2019.07.010>.
- [100] S. Mappoli, K. Ghosh, M. Pumera, MXene and polyaniline coated 3D-printed carbon electrode for asymmetric supercapacitor, *Virtual Phys. Prototyp.* 19 (2024) e2361139, <https://doi.org/10.1080/17452759.2024.2361139>.
- [101] B.K. Deka, A. Hazarika, G.-H. Kang, Y.J. Hwang, A.P. Jaiswal, D. Chan Kim, Y.-B. Park, H.W. Park, 3D-Printed structural supercapacitor with MXene-N@Zn-Co selenide nanowire based woven carbon Fiber electrodes, *ACS Energy Lett.* 8 (2023) 963–971, <https://doi.org/10.1021/acsenergylett.2c02505>.
- [102] S.A. Thomas, R.K. Mishra, A. Baby, S.P. Balakrishnan, D.N. Rajendran, J. Cherussery, Translation of supercapacitor technology from laboratory scale to commercialization, in: *Supercapacitors*, Elsevier, 2024, pp. 371–395, <https://doi.org/10.1016/B978-0-443-15478-2.00004-8>.
- [103] J. Huang, Y. Xie, Y. You, J. Yuan, Q. Xu, H. Xie, Y. Chen, Rational design of electrode materials for advanced supercapacitors: from lab research to commercialization, *Adv. Funct. Mater.* 33 (2023) 2213095, <https://doi.org/10.1002/adfm.202213095>.
- [104] R. Kötz, M. Carlen, Principles and applications of electrochemical capacitors, *Electrochim. Acta* 45 (2000) 2483–2498, [https://doi.org/10.1016/S0013-4686\(00\)00354-6](https://doi.org/10.1016/S0013-4686(00)00354-6).
- [105] M. Horn, J. MacLeod, M. Liu, J. Webb, N. Motta, Supercapacitors: a new source of power for electric cars? *Econ. Anal. Pol.* 61 (2019) 93–103, <https://doi.org/10.1016/j.eap.2018.08.003>.
- [106] S. Nahiriak, A. Ray, B. Saruhan, Challenges and future prospects of the MXene-Based materials for energy storage applications, *Batteries* 9 (2023) 126, <https://doi.org/10.3390/batteries9020126>.
- [107] N. Sun, Z. Guan, Q. Zhu, B. Anasori, Y. Gogotsi, B. Xu, Enhanced ionic accessibility of flexible MXene electrodes produced by natural sedimentation, *Nano-Micro Lett.* 12 (2020) 89, <https://doi.org/10.1007/s40820-020-00426-0>.
- [108] R. Garg, A. Agarwal, M. Agarwal, A review on MXene for energy storage application: effect of interlayer distance, *Mater. Res. Express* 7 (2020) 022001, <https://doi.org/10.1088/2053-1591/ab750d>.
- [109] S. Kajiyama, L. Szabova, K. Sodeyama, H. Iinuma, R. Morita, K. Gotoh, Y. Tatemaya, M. Okubo, A. Yamada, Sodium-ion intercalation mechanism in MXene nanosheets, *ACS Nano* 10 (2016) 3334–3341, <https://doi.org/10.1021/acsnano.5b06958>.
- [110] Z. Fan, Y. Wang, Z. Xie, D. Wang, Y. Yuan, H. Kang, B. Su, Z. Cheng, Y. Liu, Modified MXene/Holey graphene films for advanced supercapacitor electrodes with superior energy storage, *Adv. Sci.* 5 (2018) 1800750, <https://doi.org/10.1002/advs.201800750>.
- [111] S.A. Zahra, M.M. Murshed, U. Naeem, T.M. Gesing, S. Rizwan, Cation-assisted self-assembled pillared V₂CT MXene electrodes for efficient energy storage, *Chem. Eng. J.* 474 (2023) 145526, <https://doi.org/10.1016/j.cej.2023.145526>.
- [112] P.A. Shinde, A.M. Patil, S. Lee, E. Jung, S. Chan Jun, Two-dimensional MXenes for electrochemical energy storage applications, *J. Mater. Chem. A* 10 (2022) 1105–1149, <https://doi.org/10.1039/DITA04642J>.
- [113] S. Kumar, N. Kumari, T. Singh, Y. Seo, Shielding 2D MXenes against oxidative degradation: recent advances, factors and preventive measures, *J. Mater. Chem. C* 12 (2024) 8243–8281, <https://doi.org/10.1039/D4TC00884G>.
- [114] P. Forouzandeh, S.C. Pillai, MXenes-based nanocomposites for supercapacitor applications, *Curr. Opin. Chem. Eng.* 33 (2021) 100710, <https://doi.org/10.1016/j.coche.2021.100710>.
- [115] S. Zhang, N. Pan, Supercapacitors performance evaluation, *Adv. Energy Mater.* 5 (2015) 1401401, <https://doi.org/10.1002/aenm.201401401>.
- [116] S. Nanda, S. Ghosh, T. Thomas, Machine learning aided cyclic stability prediction for supercapacitors, *J. Power Sources* 546 (2022) 231975, <https://doi.org/10.1016/j.jpowsour.2022.231975>.
- [117] H. Su, S. Lin, S. Deng, C. Lian, Y. Shang, H. Liu, Predicting the capacitance of carbon-based electric double layer capacitors by machine learning, *Nanoscale Adv.* 1 (2019) 2162–2166, <https://doi.org/10.1039/C9NA00105K>.
- [118] S. Iravani, A. Khosravi, E. Nazarzadeh Zare, R.S. Varma, A. Zarrabi, P. Makvandi, MXenes and artificial intelligence: fostering advancements in synthesis techniques and breakthroughs in applications, *RSC Adv.* 14 (2024) 36835–36851, <https://doi.org/10.1039/DRA06384H>.
- [119] J.D. Gouveia, T.L.P. Galvão, K. Iben Nassar, J.R.B. Gomes, First-principles and machine-learning approaches for interpreting and predicting the properties of MXenes, *Npj 2D Mater Appl* 9 (2025) 8, <https://doi.org/10.1038/s41699-025-00529-5>.
- [120] S. Yi, L. Wang, X. Zhang, C. Li, Y. Xu, K. Wang, X. Sun, Y. Ma, Recent advances in MXene-based nanocomposites for supercapacitors, *Nanotechnology* 34 (2023) 432001, <https://doi.org/10.1088/1361-6528/ace8a0>.
- [121] A.G. Saad, A. Emad-Eldeen, W.Z. Tawfik, A.G. El-Deen, Data-driven machine learning approach for predicting the capacitance of graphene-based supercapacitor electrodes, *J. Energy Storage* 55 (2022) 105411, <https://doi.org/10.1016/j.est.2022.105411>.
- [122] A. Chenwittayakachon, K. Jitapunkul, B. Nakpalad, P. Worrayotkovit, S. Namuangruk, P. Sirisundomkit, P. Iamprasertkun, Machine learning approach to understanding the ‘synergistic’ pseudocapacitive effects of heteroatom doped graphene, *2D Mater.* 10 (2023) 025003, <https://doi.org/10.1088/2053-1583/aca8d8>.
- [123] B. Mustafa, W. Lu, Z. Wang, F. Lian, A. Shen, B. Yang, J. Yuan, C. Wu, Y. Liu, W. Hu, L. Wang, G. Yu, Ultrahigh energy and power densities of d-MXene-Based symmetric supercapacitors, *Nanomaterials* 12 (2022) 3294, <https://doi.org/10.3390/nano12193294>.
- [124] R. Garg, N.R. Patra, S. Samal, S. Babbar, K. Parida, A review on accelerated development of skin-like MXene electrodes: from experimental to machine learning, *Nanoscale* 15 (2023) 8110–8133, <https://doi.org/10.1039/D2NR05969J>.
- [125] J. Kim, J.H. Ryu, M. Jang, S. Park, M. Kim, K.H. Lee, S. Choi, Y. Yoon, H. Jung, S. S. Lee, K. An, One-dimensional π-D conjugated coordination polymer intercalated MXene compound for high-performance supercapacitor electrode, *Small Methods* 7 (2023) 2201539, <https://doi.org/10.1002/smtd.202201539>.
- [126] S. Zhu, J. Li, L. Ma, C. He, E. Liu, F. He, C. Shi, N. Zhao, Artificial neural network enabled capacitance prediction for carbon-based supercapacitors, *Mater. Lett.* 233 (2018) 294–297, <https://doi.org/10.1016/j.mattlet.2018.09.028>.
- [127] H. Mou, Z. Luo, X. Zhang, A magnetic-field-driven neuristor for spiking neural networks, *Appl. Phys. Lett.* 122 (2023) 250601, <https://doi.org/10.1063/5.0158341>.
- [128] X. Liu, X. Liu, Regression trees on grassmann Manifold for adapting reduced-order models, *AIAA J.* 61 (2023) 1318–1333, <https://doi.org/10.2514/1.J062180>.
- [129] L. Tian, W. Wu, T. Yu, Graph random forest: a graph embedded algorithm for identifying highly connected important features, *Biomolecules* 13 (2023) 1153, <https://doi.org/10.3390/biom13071153>.

- [130] H.S. Seung, M. Opper, H. Sompolinsky, Query by committee, in: Proceedings of the Fifth Annual Workshop on Computational Learning Theory, ACM, Pittsburgh Pennsylvania USA, 1992, pp. 287–294, <https://doi.org/10.1145/130385.130417>.
- [131] S.M. Pillay, I. Sinayskiy, E. Jembere, F. Petruccione, A multi-class quantum kernel-based classifier, *Adv. Quantum Technol.* 7 (2024) 2300249, <https://doi.org/10.1002/qute.202300249>.
- [132] N. Wichitaksorn, Y. Kang, F. Zhang, Random feature selection using random subspace logistic regression, *Expert Syst. Appl.* 217 (2023) 119535, <https://doi.org/10.1016/j.eswa.2023.119535>.
- [133] J. Engländer, G. Iacobelli, G. Pete, R. Ribeiro, Structural results for the tree builder random walk, <https://doi.org/10.48550/ARXIV.2311.18734>, 2023.
- [134] S. Ghosh, G.R. Rao, T. Thomas, Machine learning-based prediction of supercapacitor performance for a novel electrode material: cerium oxynitride, *Energy Storage Mater.* 40 (2021) 426–438, <https://doi.org/10.1016/j.ensm.2021.05.024>.
- [135] M. Rahimi, M.H. Abbaspour-Fard, A. Rohani, A multi-data-driven procedure towards a comprehensive understanding of the activated carbon electrodes performance (using for supercapacitor) employing ANN technique, *Renew. Energy* 180 (2021) 980–992, <https://doi.org/10.1016/j.renene.2021.08.102>.
- [136] L. Wang, S. Gao, W. Li, A. Zhu, H. Li, C. Zhao, H. Zhang, W.-H. Wang, W. Wang, Machine learning assisted screening of MXenes pseudocapacitive materials, *J. Power Sources* 564 (2023) 232834, <https://doi.org/10.1016/j.jpowsour.2023.232834>.